© 2016. Published by The Company of Biologists Ltd | Development (2016) 143, 133-146 doi:10.1242/dev.124180

RESEARCH ARTICLE

# The apical complex protein Pals1 is required to maintain cerebellar progenitor cells in a proliferative state

**Jun Young Park[1], Lucinda J. Hughes[1,2], Uk Yeol Moon[1], Raehee Park[1], Sang-Bae Kim[3], Khoi Tran[1], Ju-Seog Lee[3], Seo-Hee Cho[1] and Seonhee Kim[1,*]**

## ABSTRACT

Through their biased localization and function within the cell, polarity complex proteins are necessary to establish the cellular asymmetry required for tissue organization. Well-characterized germinal zones, mitogenic signals and cell types make the cerebellum an excellent model for addressing the crucial function of polarity complex proteins in the generation and organization of neural tissues. Deletion of the apical polarity complex protein Pals1 in the developing cerebellum results in a remarkably undersized cerebellum with disrupted layers in poorly formed folia and strikingly reduced granule cell production. We demonstrate that Pals1 is not only essential for cerebellum organogenesis, but also for preventing premature differentiation and thus maintaining progenitor pools in cerebellar germinal zones, including cerebellar granule neuron precursors in the external granule layer. In the *Pals1* mouse mutants, the expression of genes that regulate the cell cycle was diminished, correlating with the loss of the proliferating cell population of germinal zones. Furthermore, enhanced Shh signaling through activated Smo cannot overcome impaired cerebellar cell generation, arguing for an epistatic role of Pals1 in proliferation capacity. Our study identifies Pals1 as a novel intrinsic factor that regulates the generation of cerebellar cells and Pals1 deficiency as a potential inhibitor of overactive mitogenic signaling.

**KEY WORDS: Cerebellar development, Pals1, Mpp5, Polarity complex proteins, Germinal zones, Mouse, Bergmann glia**

## INTRODUCTION

A mature cerebellum includes Purkinje cells (PCs), cerebellar granule neurons (CGNs), deep cerebellar nuclei neurons (DCNs), interneurons and glial cells. Most cerebellar cells originate in two germinal zones: the ventricular zone (VZ), which is the lining of the apical cerebellar neuroepithelium; and the upper rhombic lip (URL), which is the neuroepithelium located between the cerebellar plates and choroid plexus (CP) of the fourth ventricle (Millen and Gleeson, 2008; Zervas et al., 2005). GABAergic interneurons in DCNs, PCs, interneurons and most glial cells develop from the VZ, either directly or via intermediate progenitors in the white matter. The URL and its descendants generate glutamatergic neurons in DCNs, unipolar brush cells and cerebellar granule neuron precursors (CGNPs) (Chen et al., 2013). Intricate directional movements from germinal zones organize cells in the cerebellar cortex into folia with distinct layers, including the cell-sparse molecular layer, PC layer (PCL) and granule cell layer (Roussel and Hatten, 2011).

Unlike other neurogenic areas in the developing brain, CGNPs in the external granule layer (EGL) remain proliferative throughout early postnatal ages, producing CGNs that migrate inwardly to form the inner granule cell layer (IGL). CGNPs expand progenitor pools through cell division that is mainly symmetric, and clonally related progenitors exit the cell cycle during a defined period of time (Espinosa and Luo, 2008). The PC plate beneath the EGL serves as a major source of the mitogenic signal Shh, which drives CGNP proliferation. While migrating through the Shh-rich EGL toward PCs, CGNPs exit the cell cycle and differentiate, demonstrating the exquisite balance between proliferation and differentiation that is required to coordinate CGNP clonal expansion and granule neuron generation. Overactive Shh signaling characterizes one of the four molecular subgroups of medulloblastoma, the most common malignant brain tumor in children, and occurs in ∼25-30% of cases, making this signaling pathway an attractive target for novel therapeutics (Roussel and Robinson, 2013; Taylor et al., 2012). Therefore, to further understand pathological conditions, it is crucial to investigate the cellular/molecular mechanisms that act during granule cell development to initiate differentiation in preference to proliferation in the presence of mitotic/morphogenetic signals.

Cell polarity, which comprises both molecular and cytoarchitectural asymmetry within the cell, is crucial for various cellular processes, including proliferation, differentiation and directed growth and migration. Polarity complexes include evolutionarily conserved apical complex proteins, such as the Crb complex (comprising Crbs, Pals1, Patj), the Par complex (Par3, Par6, aPKC) and basal complex proteins, such as the Scribble complex (Scribbles, Lgl, Dlg) (Assémat et al., 2008; Pieczynski and Margolis, 2011; Tepass, 2012). Previous studies have demonstrated that apical complex proteins are necessary for self-renewal of neural progenitor cells (Bultje et al., 2009; Costa et al., 2008; Kim et al., 2010), neuronal migration (Famulski et al., 2010; Solecki et al., 2006), axon determination (Chen et al., 2013; Shi et al., 2003), dendrite development (Tanabe et al., 2010), tissue polarity (Cho et al., 2012) and neuron survival (Kim et al., 2010). However, there is little information about the function of apical complex proteins in the regulation of proliferation and differentiation of CGNPs, which lack typical apical-basal polarity.

Here, we genetically ablate *Pals1* (*Mpp5* – Mouse Genome Informatics), a central component of apical complexes, in CGNPs and provide evidence that Pals1 is crucial for proliferation. Furthermore, Pals1 deficiency causes premature differentiation of cerebellar progenitors and significantly compromises the expression of genes required for cell cycle progression. Constitutively active Shh signaling in the *Pals1* mutant does not

[1]Shriners Hospitals Pediatric Research Center, Department of Anatomy and Cell Biology, Temple University School of Medicine, Philadelphia, PA 19140, USA. [2]Graduate Program of Biomedical Sciences, Temple University School of Medicine, Philadelphia, PA 19140, USA. [3]Department of Systems Biology, University of Texas MD Anderson Cancer Center, Houston, TX 77030, USA.

*Author for correspondence (seonhee.kim@temple.edu)

**Received 14 March 2015; Accepted 25 November 2015**

Development (2016) 143, 133-146 doi:10.1242/dev.124180

restore cerebellar cells, suggesting an essential Pals1 function in cellular fitness for proliferation. Together, these newly described functions identify Pals1 as a crucial intrinsic factor for regulating CGNP proliferation.

## RESULTS

### Pals1 is expressed in progenitors during cerebellar development

To study the function of Pals1 in mouse cerebellum development, we examined its expression pattern and subcellular localization. We first studied *Pals1* transcripts at E15.5 in germinal zones of the developing cerebellum (Fig. 1A). *In situ* hybridization analysis shows *Pals1* expression in these proliferating zones in wild type (WT) (Fig. 1B), and a substantial reduction upon *Pals1* deletion with *hGFAP-Cre* (see below; Fig. 1C). Beginning at E13.5, *hGFAP-Cre* was expressed in proliferating progenitors in the EGL, URL and VZ, which therefore excludes expression in early-born neurons, including PCs (Zhuo et al., 2001). Prominent expression remained in the CP, where Cre is not expressed (Fig. 1B′,C′, red arrow), which confirms deletion from the

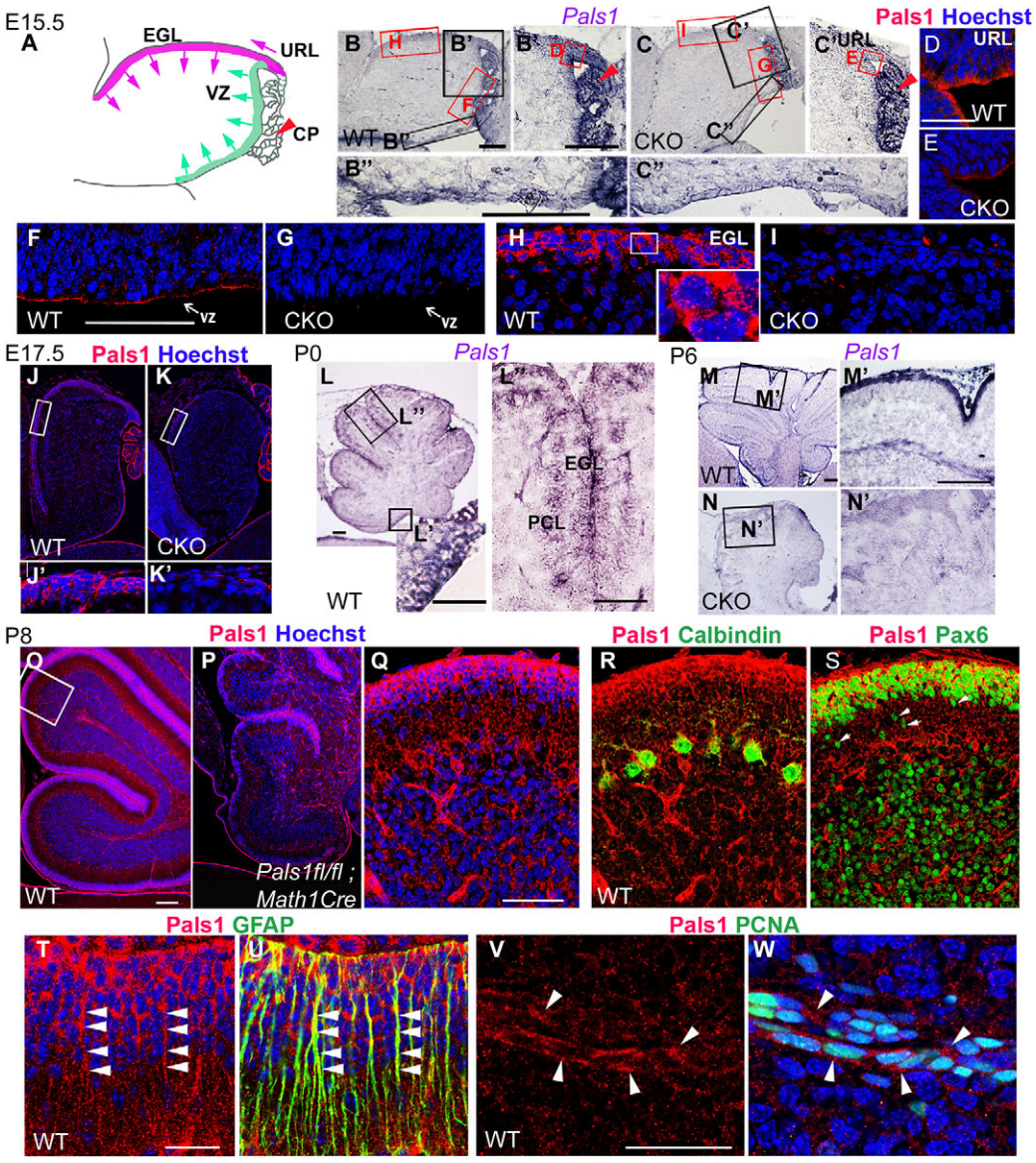


**Fig. 1. Pals1 is expressed in multiple cell types during development of the cerebellum.** (A) Schematic of VZ, URL and EGL in the developing mouse cerebellum. Arrows indicate direction of migrating cells produced from germinal zones. (B-C″) *Pals1* mRNA expression in URL, EGL, VZ and CP in WT (B-B″) and *Pals1* CKO (C-C″) mice at E15.5. Red arrowhead indicates *Pals1* expression in CP in both WT and CKO. (D-I) At E15.5 Pals1 protein is highly expressed at the apical ventricular surface of URL and VZ, and is found in the cytoplasm in EGL cells of WT (D,F,H inset); expression is diminished in *Pals1* CKO (E,G,I). (J-K′) Continued expression of Pals1 protein in URL, EGL and VZ at E17.5 in WT (J,J′), but a marked reduction in the *Pals1* CKO (K,K′). (L-L″) At P0, *Pals1* transcripts are found in ventricular lining cells (L′), EGL and PCL (L″). (M-N′) At P6 *Pals1* transcripts are prominent and concentrated in the EGL, and weak expression is seen in the white matter and PCL; *Pals1* transcripts are greatly diminished in the CKO. (O-S) At P8 Pals1 protein is detected in the EGL and PCL, including PCs, of WT. The concentrated Pals1 staining in the EGL of WT (O,Q) is not seen in lobes 1 and 2 of the EGL of the *Pals1* mutant with *Math1-Cre* (P). The boxed region in O is magnified in Q-S. Pals1 staining overlaps with calbindin in the PCL (R) and with Pax6 in the EGL (S) but $Pax6^{+}$ cells migrating out of the EGL do not show Pals1 expression (arrows). (T-W′) Pals1 expression is also detected at P8 in $Gfap^{+}$ glia processes (T,U) and $Pcna^{+}$ progenitor cells in the white matter (V,W) of cerebellum. Arrowheads indicate Pals1 expression in the cytoplasm of progenitor cells. VZ, ventricular zone; URL, upper rhombic lip; PCL, Purkinje cell layer; EGL, external granular layer; CP, choroid plexus. Scale bars: 100 µm in B-C″,L′,L″,O,P; 200 µm in L,M; 50 µm in F-I,M′,N′,Q-S; 25 µm in D,E,T-W.

Development (2016) 143, 133-146 doi:10.1242/dev.124180

cerebellum and validates the specificity of the *Pals1* probe. In accordance with known neuroepithelium expression patterns (Ishiuchi et al., 2009; Kim et al., 2010), Pals1 proteins also localized to the apical surface in the URL and VZ of WT (Fig. 1D,F). Intriguingly, Pals1 was also densely distributed in the cytoplasm of EGL cells in WT at E15.5 and E17.5 (Fig. 1H-K′). Pals1 expression in both the apical surface and cytoplasm of cerebellar cells was validated by their loss in mutant tissue. Furthermore, *Pals1* expression in ventricular apical lining cells continued at P0 (Fig. 1L,L′), when proliferating cells are almost absent from the VZ. *Pals1* was consistently observed in the proliferating EGL, and expression began in the PCL (Fig. 1L″). *Pals1* transcripts were also detected in WT at P6 and were markedly reduced in the *Pals1* mutant (Fig. 1M-N′).

Pals1 antibody staining in WT and in another *Pals1* conditional knockout (CKO) at P8 confirmed the EGL-specific cytoplasmic localization and reduction in the CKO mice (Fig. 1O,P). In this case, *Pals1* was deleted using *Math1-Cre* (*Math1* is also known as *Atoh1*), which was expressed primarily in CGNPs but not in other progenitors. Pals1 expression in PCs was determined by overlapping Pals1 and calbindin staining (Fig. 1R). Interestingly, whereas dense cytoplasmic Pals1 staining in CGNPs remained at P8, Pals1 expression was reduced in $Pax6^{+}$ postmitotic granule neurons migrating out of the EGL (Fig. 1S). Some Bergmann glia (BG) processes labeled by glial fibrillary acidic protein (Gfap) immunostaining also overlapped with Pals1, and proliferating cell nuclear antigen $(Pcna)^{+}$ progenitor cells in the white matter expressed cytoplasmic Pals1 (Fig. 1T-W′) at P8. Although the level of Pals1 in these cells was lower than in other cell types, diminished expression in the *Pals1* mutant validates its presence (Fig. S1).

Together, these observations suggest that Pals1 might serve a crucial function in the proliferation of progenitor cells in all germinal zones and in the development of PCs and BG.

## Pals1 is required for cerebellar histogenesis and foliation

The orderly generation of neurons and glia is essential to establish the cytoarchitecture and circuitry necessary for cerebellar functions (Sudarov et al., 2011). To investigate the function of Pals1 in cerebellum development, we generated a mutant with loss-of-function in most cerebellar neurons and glia using *hGFAP-Cre* mice (termed *Pals1* CKO). *Pals1* deletion resulted in a dramatically undersized cerebellum beginning at P0 (Fig. 2A-F). To characterize the cerebellar phenotype, size differences between WT and CKO were compared by measuring the length, width and circumference at the midsagittal section of the cerebellum at P0, P5 and P21 (Fig. 2A-K). Except for cerebellar width at P0, the measurements were considerably smaller in the CKO, indicating an essential function of Pals1 in cerebellum growth.

To investigate defects in layer formation and foliation, we conducted serial histological analyses at embryonic and postnatal stages (Fig. 2L-S). Phenotypic differences in the *Pals1* CKO first became noticeable at E17.5, although gross anatomical changes were absent. URL length and thickness were decreased in the *Pals1* CKO, and the dorsal surface of the cerebellar anlage, where CGNPs reside, was hypocellular (Fig. 2L′,M′). In addition, cells in the apical lining of the developing cerebellum formed a thinner VZ in the *Pals1* mutant (Fig. 2L″,M″).

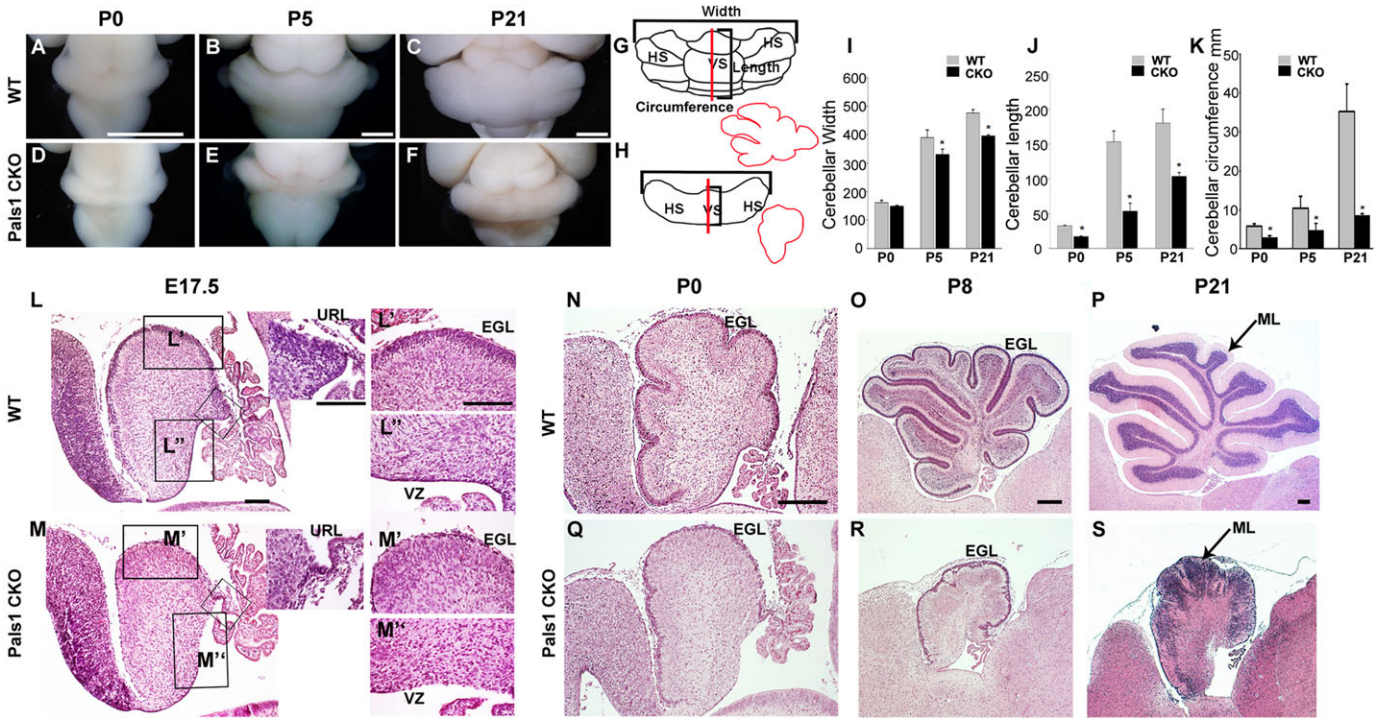


**Fig. 2. The function of Pals1 in cerebellar histogenesis.** (A-K) The *Pals1* CKO cerebellum is smaller than that of WT littermates at P0 and later. Cerebellar width, length and circumference were measured at P0 (A,D), P5 (B,E) and P21 (C,F) and *Pals1* CKO and WT were compared (G-K). Error bars indicate s.d. **P*<0.05. (L-S) Histological analysis using H&E staining. At E17.5 *Pals1* CKO mice show a diminished URL and a decreased CGNP population in the EGL (M′) compared with WT (L′). The VZ is less dense in the *Pals1* CKO (M″) than in WT (L″). At P0, cerebellar lobes have not formed in the *Pals1* CKO (Q), whereas the WT cerebellum shows 6-7 distinct lobes (N). (O,R) Deformed foliation is detected in the *Pals1* CKO (R) compared with WT (O) at P8. (P,S) An undersized cerebellum with fused lobes and a disorganized layer structure is found in *Pals1* CKO mice (S) compared with WT (P) at P21. HS, hemisphere; VS, vermis; ML, molecular layer. Scale bars: 2 mm in A-F; 100 µm in L-M″; 200 µm in N-S.

Development (2016) 143, 133-146 doi:10.1242/dev.124180

The cerebellum develops five cardinal lobes during late embryogenesis (~E18) (Sudarov and Joyner, 2007). Whereas six to seven lobes have formed at the WT vermis by P0, foliation was indistinct in the *Pals1* CKO (Fig. 2N,Q). Small indentations that indicate the sites of future fissures began to form in the surface of the cerebellum a few days later, although fissure formation was severely defective. At P8 and P21, most *Pals1* CKO animals had developed poorly layered, smaller lobes containing dispersed CGNs (Fig. 2O-S). In addition to the reduction in overall size, the incomplete elaboration of folia and absence of distinct fissures, granule cell numbers were strikingly reduced (Fig. 2R,S). In summary, histological analysis revealed an essential function of Pals1 in cerebellar histogenesis and organization.

### Pals1 is required for cerebellar layer organization

To determine the extent of the defects in cellular organization in the *Pals1* CKO, in which *Pals1* is not deleted in PCs, we first examined PC positioning and dendrite development during embryonic and postnatal stages. At P0, PCs were more broadly distributed in the white matter of the *Pals1* mutant than in WT (Fig. 3A,B). By P6, PCs remained in clusters in the *Pals1* mutant and failed to organize the PC plate into a few cell layers, as seen in WT (Fig. 3C-D′). A striking depletion of CGNPs with subsequent reduction of CGN generation in the EGL (a prime source of reelin) indicated that reelin-Dab1 signaling, which is crucial for PC migration, was compromised in the *Pals1* mutant (Fig. S2). In the *Pals1* mutant at P21, most PCs were dispersed in the cortical area and failed to form a PCL consisting of BG and PCs. Furthermore, PC dendrites appeared to be randomly directed and less elaborated than in WT (Fig. 3E-H). Defects in BG number and location, the paucity of interneurons and profound reduction of CGNs, whose axons provide synaptic inputs to PCs, may all impact development of PC dendrites in the mutant.

We next examined cerebellar BG, which are unique glial cells characterized by unipolar radial glial processes (Mason et al., 1988). In the WT, many BLBP$^+$ glial cells (BLBP is also known as Fabp7) were located beneath the EGL and formed a distinct single layer within the PCL by P6 (Fig. 3I,K). Interestingly, Pals1-deficient glia were not only decreased in number, but also remarkably dispersed throughout the cerebellar plate and even found on the pial surface at P0 (Fig. 3I,J, arrows) and thereafter (Fig. 3K-N). Additionally, radial fibers were not normally extended as in WT, but were short, stunted and bent (Fig. 3M,N, insets; Fig. S3A,B). Glial defects are likely to contribute to the disrupted IGL formation by failing to support inward radial migration of CGNs at later stages, resulting in the majority of Pax6$^+$ CGNs remaining above the PCs at adult stage (P21) (Fig. 3O-R′, shown by Nissl staining; Fig. S3C-F). Interestingly, in the *Pals1* mutants during early postnatal stages, such as P8, clusters of Pax6$^+$

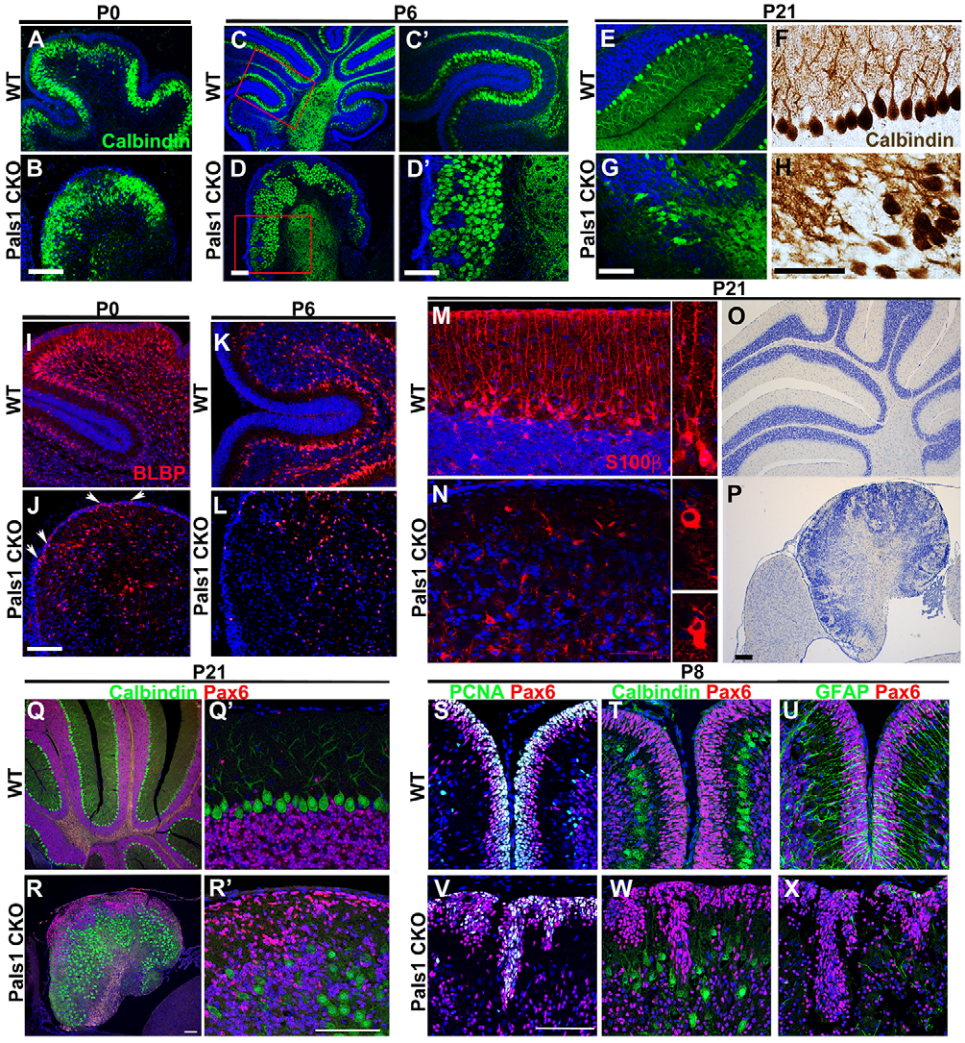


**Fig. 3. Pals1 deficiency causes lamination defects.** (A-D′) At P0 and P6, PC localization is severely disrupted in the CKO because many cells fail to reach the PCL; some remain in the deeper layer (B,D, D′), whereas PCs form a few cell layers by P6 in the WT (C,C′). (E-H) At P21, most PCs are dispersed in the cortical area and fail to form the PCL. PC dendrite processes in the CKO are less elaborated and directional (G, H) than in WT (E,F). (I,J) At P0, fewer BLBP$^+$ cells are in the cerebellum of the CKO than in WT, and some are detected underneath the pia (J, arrows). (K,L) At P6, many BLBP$^+$ glia form a layer within the PCL in WT, whereas BG in the CKO do not. (M,N) At P21, fewer S100β$^+$ cells are present in the mutant than in WT, and they are dispersed throughout the cerebellum with improperly formed radial processes. High-resolution images are shown in the insets. (O,P) Nissl staining demonstrates disorganized CGNs in CKO (P), as compared with the well-organized layer in WT (O). (Q-R′) Many Pax6$^+$ CGNs are found above the calbindin$^+$ PCs in the *Pals1* mutant. (S-X) At P8, the clusters of Pax6$^+$ Pcna$^+$ cells surrounded by Pax6$^+$ Pcna$^-$ cells are extended inward. Disorganized PCs and a few randomly directed Gfap$^+$ glial fibers are present in the *Pals1* CKO compared with WT. Scale bars: 100 µm in A-H,Q-X; 200 µm in I-P.

Development (2016) 143, 133-146 doi:10.1242/dev.124180

EGL cells, which contain Pcna$^{+}$ proliferating CGNPs, extended inward (Fig. 3S-W). It is possible that clusters were formed by CGNP cells that were detached from the EGL but remained proliferative in the cortex. Alternatively, the anchoring center at the base of the fissure might not have formed properly, resulting in defective outward growth. It has been shown that the anchoring center is initiated by differential proliferation and cell shape change of CGNPs and that PCs and BG at the base of the fissure are crucial in maintaining this structure (Sudarov and Joyner, 2007). Profound defects in these cell types in the *Pals1* mutant are therefore likely to have contributed to the unsuccessful fissure formation (Fig. 3P,R).

In summary, Pals1 loss severely affected the fissure formation and organization of cerebellar layers, as demonstrated by reduced numbers of neurons and glia and the dispersion of cerebellar cells.

### *Pals1* deletion disrupts apical complex protein localization in cerebellar neuroepithelium

To understand the cellular changes underlying the severely reduced neuronal and glial production, we examined tissue integrity and associated cellular junction proteins. At E15.5, when Pals1 protein had largely disappeared from the apical junction in the mutant (Fig. 1F,G), tissue integrity appeared to be relatively intact (Fig. 4A,E). However, when we examined changes in junctional components by marker analyses, the *Pals1* CKO showed profound reduction of ZO1 (Tjp1 – Mouse Genome Informatics) at the apical junction and reduced localization of the adherens junction components N-cadherin and β-catenin (Fig. 4B-H; data not shown).

Pals1 functions as a scaffold to recruit apical polarity complex proteins via its protein-protein interaction domains, including PDZ, SH3 and L27 (Roh et al., 2003). The scaffold assembles and maintains a macromolecular network at the apical junction. Crb transmembrane proteins, which bind with Pals1 via a PDZ-binding motif, were not localized at the apical junction in *Pals1* CKO (Fig. 4I,L,K,N). The Pals1-deficient cerebellum also did not maintain the Par complex proteins Par3 and aPKC at the apical junction (Fig. 4J,M,O,P). Defective apical localization of Crbs and Par complex proteins in the *Pals1* CKO is consistent with our previous findings in the developing cortex and retina (Kim et al., 2010; Cho et al., 2012). Comparable defects were observed in the URL (data not shown), but defects in the EGL were difficult to assess, most likely because it is challenging to detect apical polarity complexes in non-epithelial cells. Thus, our results demonstrate defective apical polarity complex protein localization in Pals1-deficient cerebellum, similar to what has been observed in cerebral cortex progenitors (Kim et al., 2010).

### Loss of Pals1 reduces ventricular progenitors, interneurons and glial cells

Since our histological analysis clearly demonstrated hypocellularity in the apical lining of VZ starting at E17.5, we determined the number of S-phase cells at the VZ after acute (30 min) BrdU labeling at E15.5, E17.5 and P0 (Fig. 5A-F). At E15.5 the percentage of BrdU$^{+}$ cells in the *Pals1* mutant did not significantly differ from that in the WT, but reductions were statistically significant at E17.5 (Fig. 5B). At P0, few BrdU$^{+}$ cells were found in the apical lining of either WT or CKO; VZ is no longer mitotically active after birth (Fig. 5B). To investigate whether cell cycle behavior is altered in Pals1-deficient cerebellum, we determined the proportion of BrdU$^{+}$ S-phase cells among total Ki67$^{+}$ dividing cells at E17.5; however, there was no statistically significant difference between CKO and WT (Fig. 5C,E). Importantly, analyses of populations exiting the cell cycle (assessed by BrdU$^{+}$ Ki67$^{-}$ cells among total BrdU$^{+}$ cells after BrdU labeling 24 h prior to harvest at E17.5) demonstrated a significantly increased fraction of exiting cells in the absence of Pals1 (Fig. 5D,F).

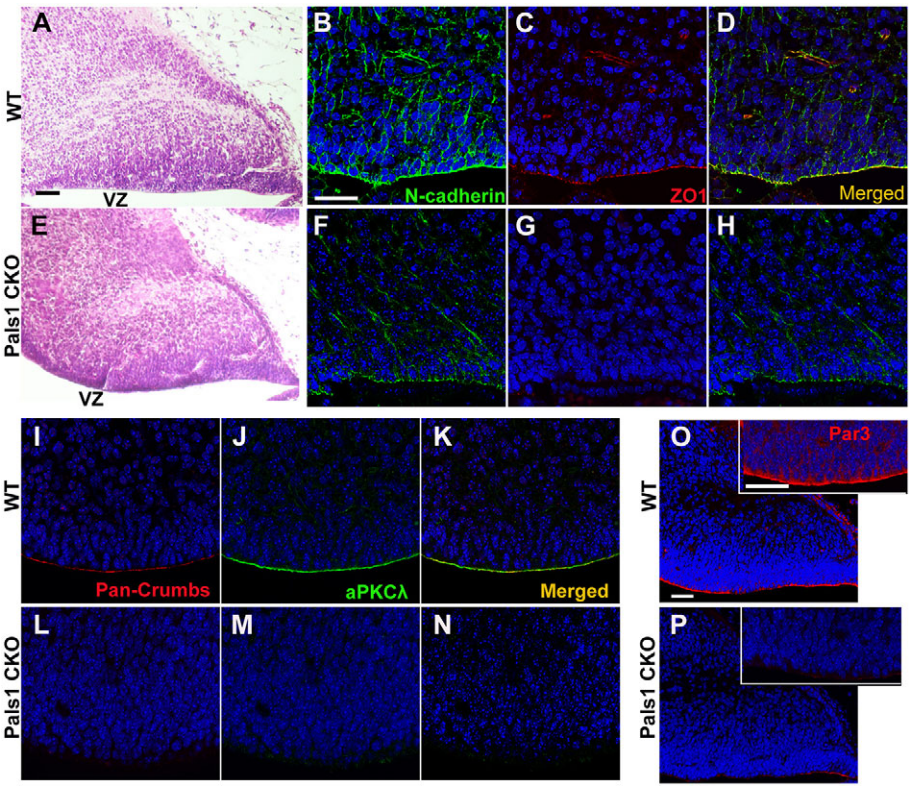


**Fig. 4. Pals1 is required for localization of apical junction proteins.** (A,E) Histological analysis at E15.5 does not reveal distinctive structural abnormalities in the *Pals1* CKO, which is comparable to WT. (B-D,F-H) The adherens junction protein N-cadherin shows some decrease, whereas ZO1 is strikingly reduced at the apical junction in the *Pals1* CKO (F-H) as compared with the WT (B-D). (I-N) Apical complex proteins, such as Crb (red) and aPKC (green), are no longer detectable at the apical junction in the *Pals1* CKO. (O,P) Par3 proteins are not well maintained at the apical junction in the *Pals1* CKO. Scale bars: 100 µm in A,E; 50 µm in B,D,F-P.

Development (2016) 143, 133-146 doi:10.1242/dev.124180

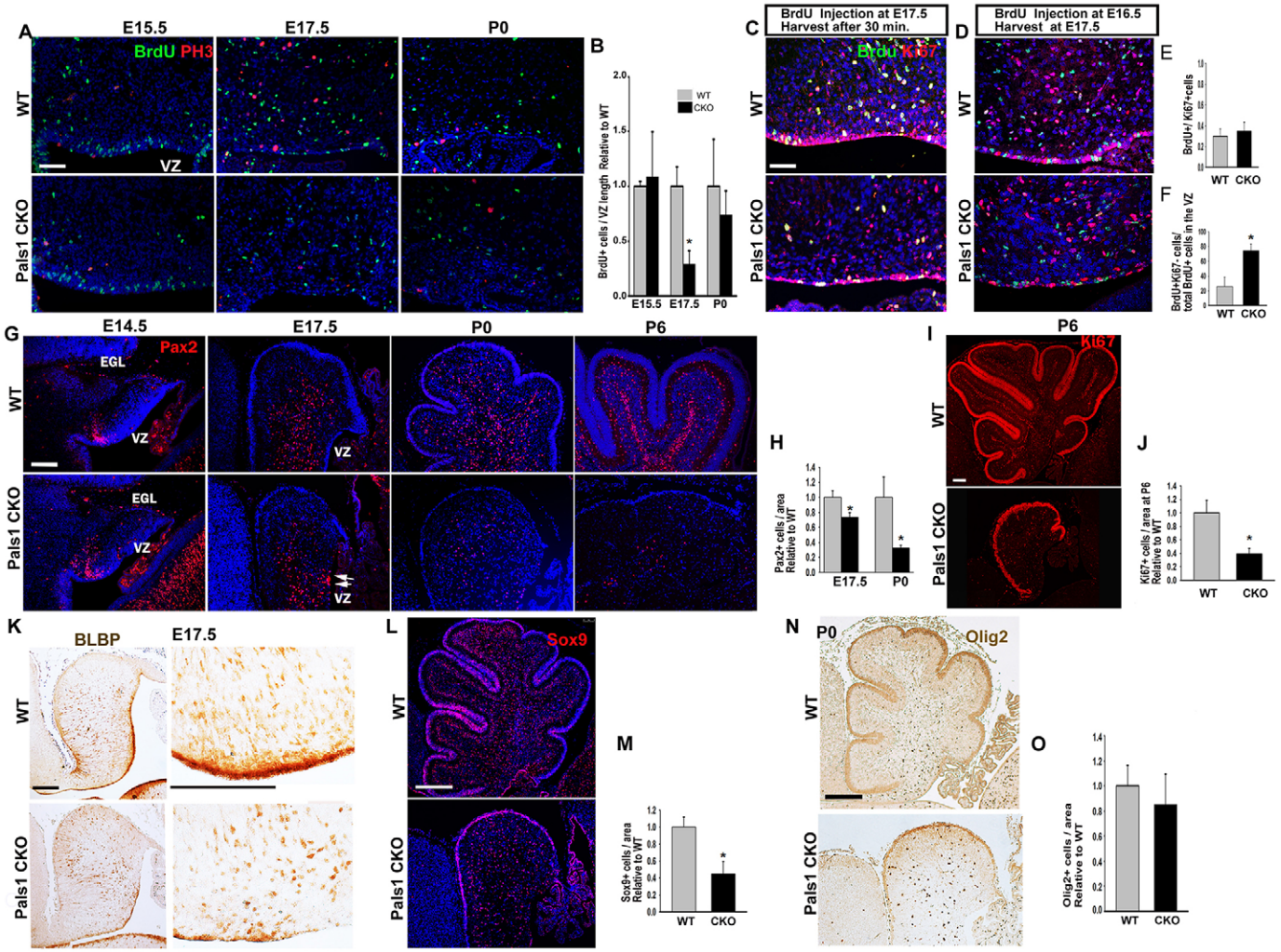


**Fig. 5. Pals1 depletion reduces proliferating VZ progenitors, interneurons, glial cells and their progenitors.** (A) Proliferative progenitors in the VZ were monitored with transient BrdU incorporation at E15.5, E17.5 and P0. (B) BrdU$^+$ cells are reduced at E17.5 and P0 in the *Pals1* CKO, but the reduction is statistically significant only at E17.5 ($n$=3, *$P$=0.0019). (C,E) The proportion of S-phase cells marked by BrdU among total progenitor cells (Ki67$^+$) in the VZ at E17.5 is slightly increased in the CKO, but the reduction is not statistically significant ($n$=3, $P$=0.2558). (D,F) The population exiting the cell cycle (BrdU$^+$/Ki67$^-$ among total BrdU$^+$) is increased in the *Pals1* CKO 24 h after BrdU administration ($n$=3, *$P$=0.0029). (G,H) GABAergic interneurons detected by Pax2 immunostaining in the CKO are reduced in number and enriched at the apical side at E17.5 (arrows), and there is a significant decrease in Pax2$^+$ cells at E17.5 ($n$=3, *$P$=0.0073) and P0 ($n$=3, *$P$=0.0249). (I,J) Ki67$^+$ cells in the cerebellum, excluding the EGL, are reduced at P6 in CKO ($n$=3, *$P$=0.0032). (K) Fewer BLBP$^+$ cells are present at E17.5 in the VZ of the *Pals1* CKO than that of WT. Enlarged images of the VZ are displayed to the right. (L,M) Sox9$^+$ cell density is significantly reduced in the *Pals1* CKO as compared with WT at P0 ($n$=3, *$P$=0.004). (N,O) Counts of Olig2$^+$ cells with area normalization in the *Pals1* CKO do not show any statistically significant change at P0 ($n$=3, $P$=0.069). Error bars indicate s.d. Scale bars: 50 µm in A,C,D; 200 µm in G,I,K,L,N; 100 µm in K enlargements.

Reduction of VZ progenitor pools and the increased cell cycle exit fraction in the *Pals1* mutant might have resulted from facilitated differentiation into cerebellar interneurons, which can be detected by transient Pax2 expression (a marker for postmitotic interneurons) in the white matter (Maricich and Herrup, 1999). Consistent with this notion, Pax2$^+$ cells were either shifted to the ventral side or located in the ventricular apical surface at E17.5 (Fig. 5G, arrows), indicating premature differentiation of VZ cells to Pax2$^+$ interneurons and/or migration defects. During the late embryonic stage and especially at P0 and P6, Pax2$^+$ cells were strikingly reduced in the white matter in *Pals1* CKO (Fig. 5G,H). It is noteworthy that parvalbumin$^+$ interneurons were also significantly decreased at P21 (Fig. S4). This suggests either that the number of VZ-derived bipotent white matter progenitor cells, which generate both glia and interneurons (Parmigiani et al., 2015), is reduced or that their proliferation is defective.

The cerebellar VZ also produces glial cells and their progenitors; these populations were severely reduced when *Pals1* was deleted. BLBP immunostaining revealed a reduction of glial cells in the cerebellar VZ of the *Pals1* CKO at E17.5, a few days after *Pals1* deletion (Fig. 5K), and the reduction was more obvious at P0 and thereafter (Fig. S5, Fig. 3I-N). Because the dramatic reduction of Pax2$^+$ interneurons and glial cells indicates depletion of progenitors, we examined the number of Sox9$^+$ progenitor cells in the white matter, excluding the EGL. As predicted, the number and density of Sox9$^+$ progenitors were reduced at P0 (Fig. 5L,M). Comparing numbers of Ki67$^+$ cells also revealed fewer proliferating cells in the white matter at P6, excluding the EGL (Fig. 5I,J). However, although Olig2$^+$ oligodendrocyte progenitors were also drastically reduced at P0, cell density remained unchanged (Fig. 5N,O). In summary, Pals1 loss results in fewer proliferating cells in the cerebellar VZ and

Development (2016) 143, 133-146 doi:10.1242/dev.124180

compromises the production of ventricular-derived progenitors, neurons and glial cells.

### Pals1 is required for CGNP production and maintenance of progenitor cells in the EGL

To determine why there were significantly fewer CGNs in the *Pals1* mutant cerebellum, we examined the production of CGNPs. The initial CGNP population is generated from the URL and from E13.5 to E18.5 migrates tangentially to the dorsal surface of the cerebellar plate underneath the pia (Wingate and Hatten, 1999). A second phase of massive amplification of CGNPs through active proliferation occurs within the EGL during the early postnatal stage (peak at P6) (Roussel and Hatten, 2011). We first examined CGNP production during embryogenesis by labeling S-phase cells with BrdU (Fig. 6A-F). In the *Pals1* mutant, the number of BrdU$^+$ CGNPs was slightly reduced at E15.5, but at E17.5, when URL shortening became apparent, the BrdU$^+$ cell fraction in the EGL was significantly diminished (Fig. 2L,M, Fig. 6B,E,G,). This reduction persisted through later stages (Fig. 6C,F,G; data not shown). Immunostaining M-phase cells for phospho-histone H3 (PH3) and phospho-vimentin (4A4), and cycling cells for the pan-progenitor marker Ki67, corroborated the findings from BrdU labeling (Fig. 6A-F, Fig. S6).

Because the stunted URL is one of the most consistent and striking features of the *Pals1* mutant cerebellum, we examined p27Kip1 (p27; Cdkn1b – Mouse Genome Informatics) expression to determine whether premature differentiation contributes to the smaller URL. Immunostaining for p27, a cell cycle inhibitor that prevents cell cycle re-entry, allows us to identify cells that have exited the cell cycle (Fig. 6H-J). Close examination revealed widespread p27-expressing cells in the stunted URL of *Pals1*-deficient mice at E17.5 (Fig. 6I′), whereas in WT intense p27 expression was limited to the central portion of the URL (Fig. 6H′, arrow). We also found that >75% of URL cells expressed p27 in the CKO, compared with only 35% in WT (Fig. 6H′,I′, boxed area in 6J). Thus, the premature depletion of URL progenitor cells observed in the *Pals1* mutant may underlie the reduction of CGNPs due to the compromised supply of URL-derived cells at later stages, which include CGNPs in the posterior lobes (Chizhikov et al., 2010; Machold and Fishell, 2005).

We next examined expression of the neural marker Tuj1 (Tubb3 – Mouse Genome Informatics) at E17.5 to investigate whether excessive neuronal differentiation reduces the CGNP population. In WT, the outer EGL domain was occupied by proliferating CGNPs and Tuj1$^+$ neurons were absent, whereas in the *Pals1* mutant Tuj1$^+$ cells almost completely occupied the EGL (Fig. 6K,L). Furthermore, comparing the distribution of Pax6$^+$ cells in the CKO with WT revealed that many Pax6$^+$ cells were not retained in the EGL, indicating precocious cell cycle exit and departure from the proliferating zone (Fig. 6M,N). Although the total number of

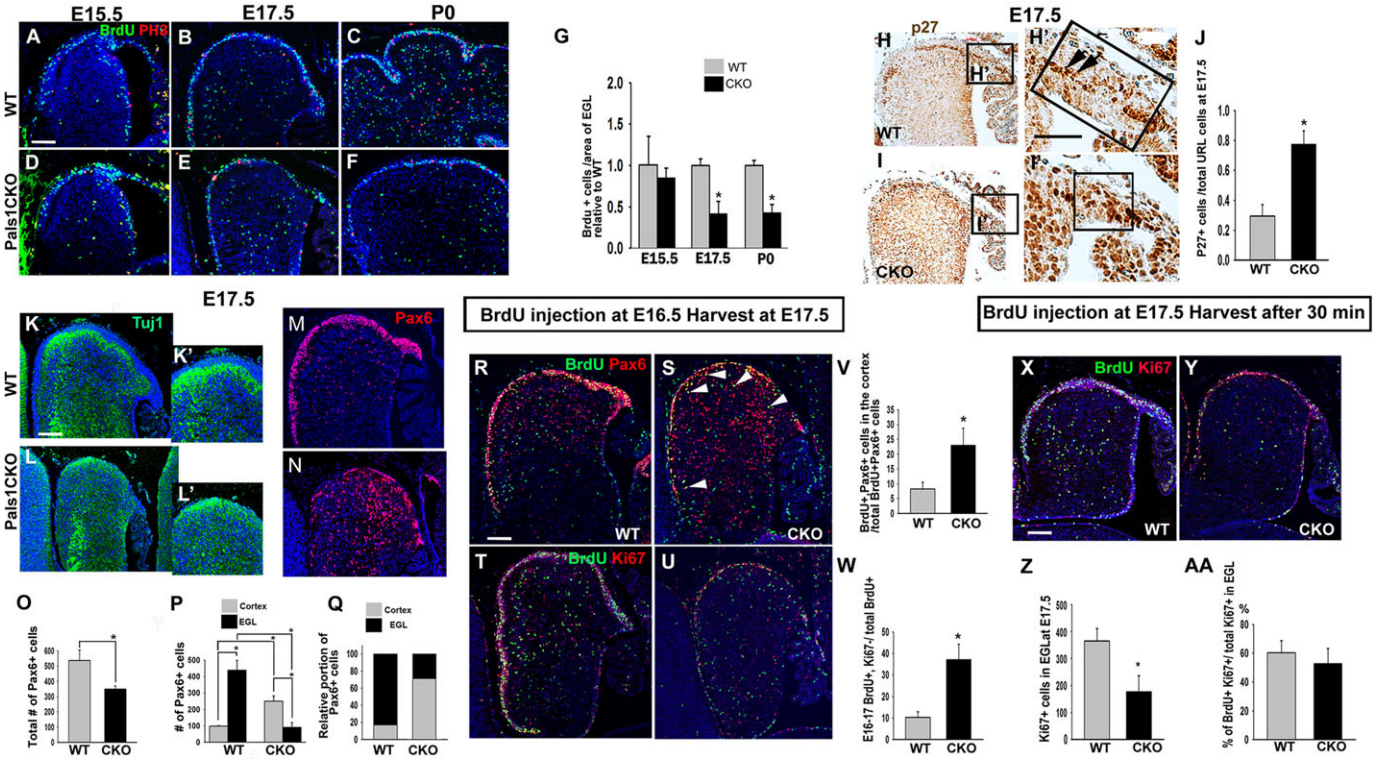


**Fig. 6. Loss of Pals1 reduces the proliferation of CGNP cells in the EGL.** (A-G) Proliferative progenitors were labeled by BrdU incorporation at E15.5, E17.5 and P0 and stained with BrdU and PH3 antibody. BrdU$^+$ CGNP cells normalized for EGL area are significantly reduced at E17.5 ($n$=3, *$P$=0.0019) and P0 ($n$=3, *$P$=0.00046) in *Pals1* CKO as compared with WT. (H-J) Cells strongly expressing p27 are lined up in the central area of the WT URL (H′, arrows), but in the CKO the p27$^+$ cells are dispersed in a short and stunted URL (I′). (J) More than 75% of CKO cells in the URL express p27, but only 35% of WT ($n$=3, *$P$=0.0001). (K-L′) Tuj1$^+$ cells (green) extend beneath the pia in the CKO, but are not present in the outer EGL of WT. (M-Q) More Pax6$^+$ cells are dispersed outside the EGL in the CKO than in WT (M,N). Fewer Pax6$^+$ cells are found in the CKO (*$P$=0.003887) (O), and their distribution is greatly shifted to a deeper area than the EGL in the CKO compared with WT ($n$=3, *$P$=0.0004) (P,Q). (R,S,V) The fraction of BrdU-labeled Pax6$^+$ cells in the cortex among total Pax6$^+$ cells is significantly increased in the CKO ($n$=3, *$P$=0.0072). Arrowheads (S) indicate BrdU-labeled Pax6$^+$ cells in the cortex. (T,U,W) The proportion of BrdU$^+$/Ki67$^-$ cells among total BrdU$^+$ cells is increased in the EGL of CKO compared with WT ($n$=3, *$P$=0.0019). (X-AA) Although progenitor cells are greatly reduced in the EGL of the CKO (Z), the portion of S-phase cells marked by 30 min (BrdU$^+$ cells among Ki67$^+$ progenitor cells) is only slightly decreased, and the decrease is not statistically significant ($n$=3, $P$=0.1915) (AA). Error bars indicate s.d. Scale bars: 100 µm.

Development (2016) 143, 133-146 doi:10.1242/dev.124180

Pax6$^+$ cells at E17.5 was 25% lower in the CKO than in WT (Fig. 6O), the number of Pax6$^+$ cells in deeper layers showed a greater than 2-fold increase compared with WT (Fig. 6P). In WT, 80% of Pax6$^+$ cells were found in the EGL, compared with only 30% in the CKO (Fig. 6Q), demonstrating the role of Pals1 in maintaining the CGNP pool in the EGL. Similar phenotypes persisted 1 day later (Fig. S7).

Because increased fractions of cells expressing p27 and Tuj1 indicated perturbation of proliferation in Pals1-deficient cerebellum, we used BrdU labeling at E16.5 followed by Ki67 staining 24 h later to investigate the fraction of EGL cells exiting the cell cycle. We first assessed the population of cells that had exited the cell cycle by determining the number of BrdU$^+$ cells among Pax6$^+$ cells that were not in the EGL (Fig. 6R,S). We found a greater than 3-fold increase in cells exiting the cell cycle in the CKO compared with WT (Fig. 6V). Next, we compared the proportion of BrdU$^+$ cells that remained in the EGL but were postmitotic, as determined by the absence of Ki67 immunostaining (Fig. 6T,U). We found an ∼4-fold increase in the exiting fraction in CKO compared with WT (Fig. 6W).

We next examined whether apoptosis plays a significant role in the substantial reduction of CGNPs in the EGL during late embryogenesis and P0. In striking contrast to the massive cell death observed in *Pals1* CKO cerebral cortex (Kim et al., 2010), the developing cerebellum showed no significant increase in dying cells at E15.5, E16.5, E17.5 or P0 (Fig. S8). An alternative explanation for the cellular loss is increased cell cycle length (slowdown of cell cycle speed). To determine whether Pals1 deficiency affects cell cycle length, we examined the proportion of S-phase cells by counting BrdU$^+$ cells among Ki67$^+$ cells after 30 min BrdU pulse labeling. We did not find any statistically significant changes in the fraction of progenitor cells in S-phase despite significantly fewer proliferating cells in the CKO (Fig. 6X-AA). This suggests that cell cycle length is not altered or that, if cell cycling speed is altered, S-phase length is changed proportionally with total cell cycle length. In summary, Pals1 may not be essential once CGNPs enter the cell cycle, but it is crucial at G1 to enter S-phase. Thus, the failure of CGNPs to remain in the cell cycle, which leads to premature differentiation, is a main contributor to reducing the number of CGNPs in the Pals1-deleted EGL.

It is possible that abnormal CGNP proliferation is a consequence of compromised BG development, as previously reported in *Ptpn11*-deficient cerebellum (Li et al., 2014). To determine whether cell-autonomous Pals1 function is required for CGNP proliferation, we used *Math1-Cre* mice to delete *Pals1* specifically in CGNPs. There was no obvious difference in the overall distribution of calbindin$^+$ PCs or S100β$^+$ BG at P0 or P22 (Fig. 7A,C,S,T). However, the anterobasal lobe (ABL) showed prominent changes in the CGNP population at P0, consistent with the location of the marked Pals1 reduction in *Math1-Cre* mice (Fig. S9). Analogous to what we found with *hGFAP-Cre* at E17.5, the reduction of progenitor cells was accompanied by premature cell cycle exit, as determined by an ∼3-fold increase in p27$^+$ cells and a corresponding loss of Ki67$^+$ cell density in the EGL of the ABL (Fig. 7B,D-F). This finding was confirmed by an increased cell cycle exit fraction, as marked by BrdU$^+$ Ki67$^-$ cells 24 h after BrdU administration at P0 (Fig. 7H-J′,L). Similar to *Pals1* loss with *hGFAP-Cre*, however, the fraction of S-phase cells among progenitor cells was not significantly different from WT (Fig. 7G, I,K). Lobe size was markedly reduced, with a decreased EGL at P8 and decreased IGL at P22 (Fig. 7M-T). Posterior lobes were relatively less affected, correlating with inefficient loss of Pals1 in that region (Fig. S9). Of note, the less severe phenotype of the mutant in which *Pals1* was deleted specifically from CGNPs, as compared with *Pals1* deletion with *hGFAP-Cre*, might also suggest that Pals1 loss in other cell types contributes to impaired CGNP proliferation. Nonetheless, specific deletion of *Pals1* in CGNPs provides evidence that Pals1 has a cell-autonomous function in CGNP proliferation.

### Expression of genes regulating cell cycle progression is reduced in the *Pals1* mutant

To determine molecular changes in Pals1-deficient cerebellum, we conducted transcriptome analyses of *Pals1* CKO with *hGFAP-Cre* and WT by microarray at E17.5, when *Pals1* deletion starts to exhibit compromised progenitor proliferation in germinal zones, including the VZ and EGL. We identified 726 genes with significantly altered expression in CKO compared with WT (fold change >±1.5, $P$<0.001); these served as user-defined focus genes for ingenuity pathway analysis. DNA replication and mitotic progression were the first and second ranked of the top ten relevant pathways (Fig. 8A, Fig. S10, Table S1). We confirmed the differential expression of 16 genes in these pathways by real-time PCR; 11 showed statistically significant differences (Fig. 8B).

We next carried out gene network analysis to identify upstream regulators of the 726 genes in the signature and discovered strong overrepresentation of E2F family members (Fig. 8C, Table S2). As expected, the vast majority of known downstream targets of E2f1 and E2f2 were significantly downregulated in *Pals1* CKO mice (Fig. 8C). Although we cannot exclude the possibility that the reduced expression of proliferation genes in this signature simply reflects the loss of progenitor populations, it is possible that Pals1 loss impairs proliferation of cerebellar progenitors by downregulation of E2F family members and their transcription targets.

### Pals1 deficiency abrogates activated Shh signaling responses

To determine whether Pals1 is epistatic to Shh signaling, we generated mice expressing the *SmoM2* allele (activated smoothened) on a *Pals1* CKO background. The *SmoM2* allele carries a mutation (W535L) found in medulloblastoma patients that causes constitutively active Shh signaling (Jeong et al., 2004). As predicted, highly activated Shh signaling in the *SmoM2*/*hGFAP-Cre* mice resulted in a hypertrophic cerebellum with overly abundant Pax6$^+$ CGNPs and CGNs, and slightly increased Pax2$^+$ interneurons at P0 (Fig. 9A,D,E,H). However, Pax2$^+$ cell density was not significantly different from WT (Fig. 9J), supporting the idea that the major target of hyperactive Shh signaling is CGNP proliferation.

Unexpectedly, the *SmoM2* allele crossed into the *Pals1* CKO did not increase the number of Pax6$^+$ and Pax2$^+$ cells at P0, and double mutants were indistinguishable from *Pals1* CKO in terms of cerebellum size and morphology (Fig. 9A-J′). However, at a later stage (P24), small regions of tissue containing a cluster of abnormal cells (Fig. 9N,N′) were apparent on the surface of the double-mutant cerebellum, which is clearly distinct from the typical *SmoM2* phenotype (Fig. 9K-M). Cells in these small clusters were labeled by Ki67, indicating that they are mitotically active (Fig. 9O). They were also immunoreactive for glial cell markers such as S100β and Gfap (Fig. 9P; data not shown), suggesting glial characteristics. This finding suggests the possibility of tumorigenic activity in the double mutant.

Development (2016) 143, 133-146 doi:10.1242/dev.124180

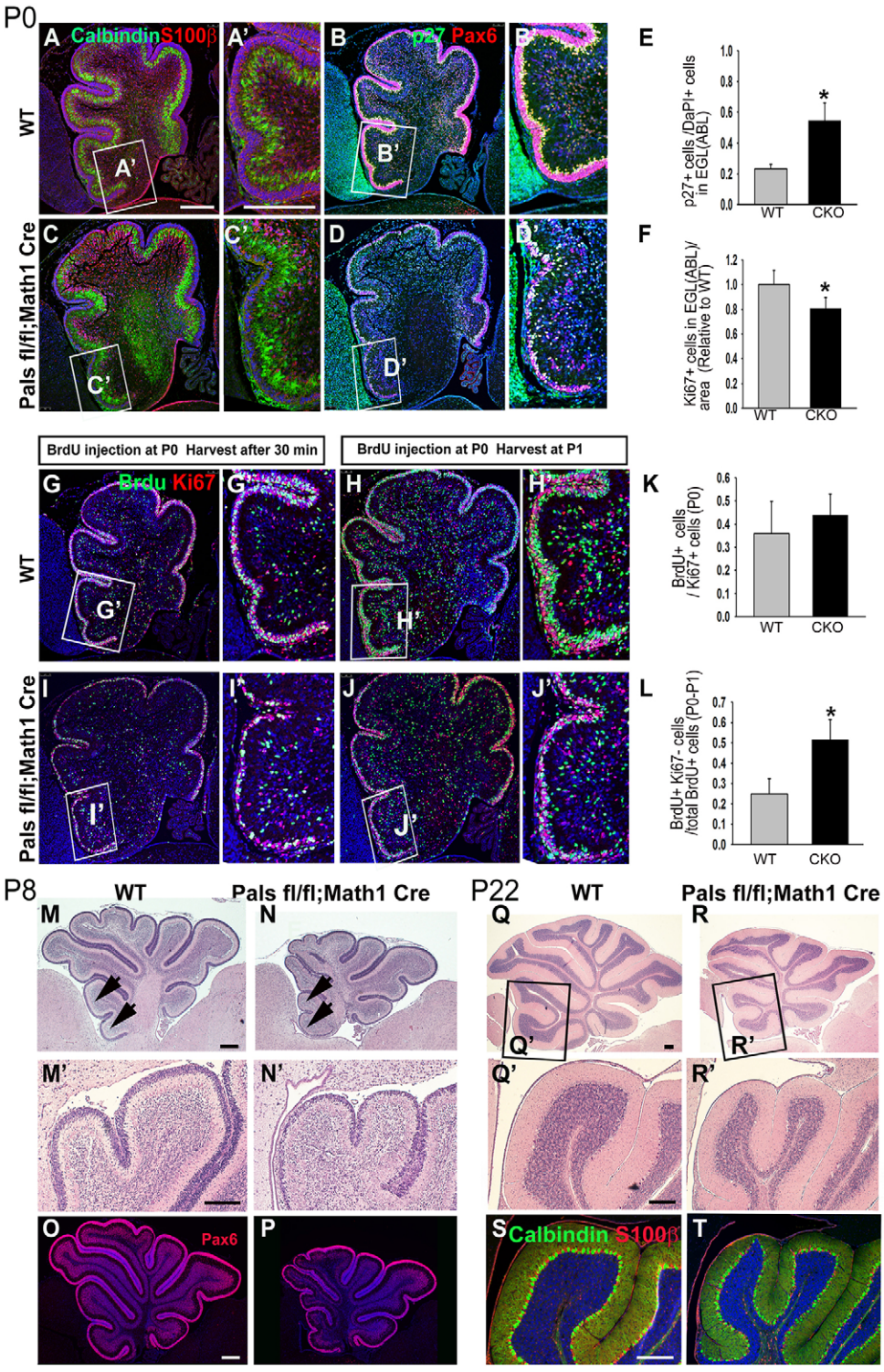


**Fig. 7. Pals1 deficiency in CGNPs causes a cell-autonomous decrease of CGNP proliferation.** (A,A′,C,C′) At P0, glial cells (S100β$^+$) and PCs (calbindin$^+$) are distributed normally in WT and *Pals1$^{fl/fl}$;Math1-Cre* animals. (B,B′,D-F) Comparison of p27$^+$ postmitotic cells or Ki67$^+$ progenitor cells after normalization of EGL area in the *Pals1$^{fl/fl}$;Math1-Cre* animals with those of WT reveals a statistically significant increase ($n$=3, *$P$=0.0034) or reduction ($n$=3, *$P$=0.0393), respectively. (G,G′,I,I′,K) The proportion of BrdU$^+$ S-phase cells among Ki67$^+$ progenitors is less affected in the EGL of the *Pals1* mutant compared with the WT ($n$=3, $P$=0.2254). (H,H′,J,J′,L) The population exiting the cell cycle (BrdU$^+$/Ki67$^-$ among total BrdU$^+$) is increased in Pals1-deficient EGL cells ($n$=3, *$P$=0.0101). (M-T) The density of EGL cells determined by histology (M-N′) or of Pax6$^+$ EGL cells at P8 (O,P) or IGL cells at P22 (Q-R′) is most prominently reduced in the anterior lobes where Pals1 expression is most effectively diminished by *Math1-Cre*. Arrows (M,N) indicate lobes 2 and 3. (S,T) PCs (calbindin$^+$) and glia (S100β$^+$) are not apparently affected in the *Pals1$^{fl/fl}$;Math1-Cre* animals. Error bars indicate s.d. Scale bars: 200 µm.

Together, our data show that Pals1 deficiency can block medulloblastoma formation despite an oncogenic mutation and suggest that the suppression of uncontrolled CGNP proliferation is due to the direct loss of Pals1 and/or the severe developmental defects that arise from its deficiency.

## DISCUSSION

Our study has demonstrated that Pals1 is required to maintain the proliferative capability of progenitors in cerebellar germinal zones regardless of epithelial polarity and that it acts by promoting cell cycle progression. Remarkably, our genetic study revealed that *Pals1* deficiency can abolish the hypertrophic effect of overactive Shh signaling, suggesting a crucial function in maintaining cells in a cycling state under normal as well as disease conditions.

### Cerebellar progenitors require Pals1 to remain in the cycling pool

Our study revealed an essential function of Pals1 in maintaining all cerebellar germinal zones, including the EGL, which produces the most abundant neurons in the mammalian brain. Although *Pals1*

Development (2016) 143, 133-146 doi:10.1242/dev.124180

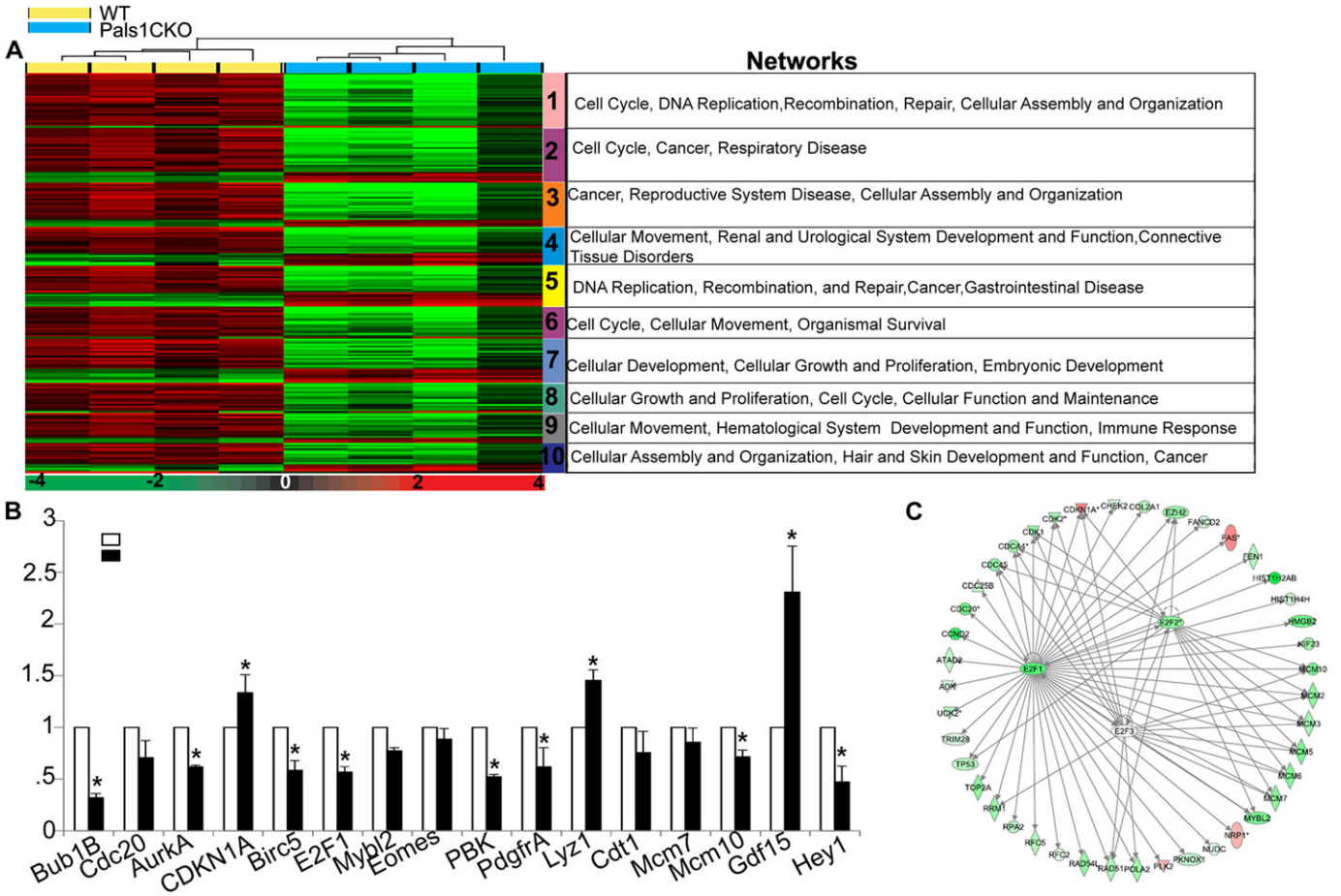


**Fig. 8. The expression of genes important for cell cycle progression is altered by loss of Pals1.** (A) Ingenuity pathway analysis identifies significantly altered networks in *Pals1* CKO based on microarray data obtained from four WT and four CKO animals at E17.5. (B) The differential expression of 16 selected genes from networks 1 and 2 is confirmed by real-time PCR (*$P$<0.05). Error bars indicate s.d. (C) Comparison of *Pals1* CKO with WT shows that expression of E2F family members and their target genes is most prominently affected.

deletion in the neuroepithelium causes near absence of cortical structure (Kim et al., 2010), Pals1 function in the proliferation of non-epithelial progenitors is unknown. During cerebellum development, Pals1 is expressed in all proliferating zones, including the VZ, URL, EGL, PCL and white matter, suggesting a possible cell-autonomous requirement in their propagation. We specifically demonstrated the cell-autonomous requirement for Pals1 in CGNP proliferation using *Math1-Cre*-mediated *Pals1* deletion, which produced a striking reduction of proliferating CGNPs through premature differentiation. This result unambiguously establishes the function of Pals1 in non-epithelial progenitor proliferation. The Pals1-deficient white matter, another non-epithelial germinal zone in the cerebellum, also showed significantly reduced progenitor populations labeled by Sox9 or Ki67. Although distinct mitogenic signals and/or cyclins are utilized in different germinal zones (Chen et al., 2013; Julian et al., 2010; Parmigiani et al., 2015), the common function of Pals1 in each germinal zone indicates that it might play a central role in cell cycle progression for all cerebellar progenitors.

Despite the reduction of the total progenitor pool in the *Pals1* mutant, the S-phase fraction of cycling cells was unchanged, suggesting that Pals1 loss forces progenitors to exit the cell cycle without obviously altering total cell cycle or S-phase lengths. Furthermore, no prominent cell death of progenitors or prematurely differentiated cells was seen, contrary to what occurs in the cerebral cortex. This suggests that Pals1 might be specifically required for G1/S transition during progenitor cell division. It is also in line with the transcriptional profiling data of the Pals1-deficient cerebellum, which revealed profoundly reduced expression of the E2F transcription factor family, which are master regulators of cell proliferation required for the G1/S transition. Although we cannot rule out the possibility that the array data simply reflect the reduction in the proliferating cell population and the corresponding increase of differentiated cells, it might imply a direct link between cell polarity protein function and proliferative capability through E2F family regulation. Intriguingly, the *C. elegans* E2F gene is implicated in establishing early embryonic polarity, a process in which apical polarity complex proteins play a major role, consistent with a functional connection (Noatynska et al., 2013; Page et al., 2001; Rabilotta et al., 2015; St Johnston and Ahringer, 2010). Our study therefore firmly establishes that Pals1 serves an essential function in the cell cycle progression of cerebellar progenitor cells, possibly by regulating the E2F family transcriptional network.

### The molecular mechanism underlying Pals1 control of progenitor cell proliferation

Our gene profiling study of the developing cerebellum did not detect any obvious changes in downstream effectors of well-established mitogenic signaling, such as Notch or Shh. In addition, the suppression of overactive Shh signaling by Pals1 loss suggests an

Development (2016) 143, 133-146 doi:10.1242/dev.124180

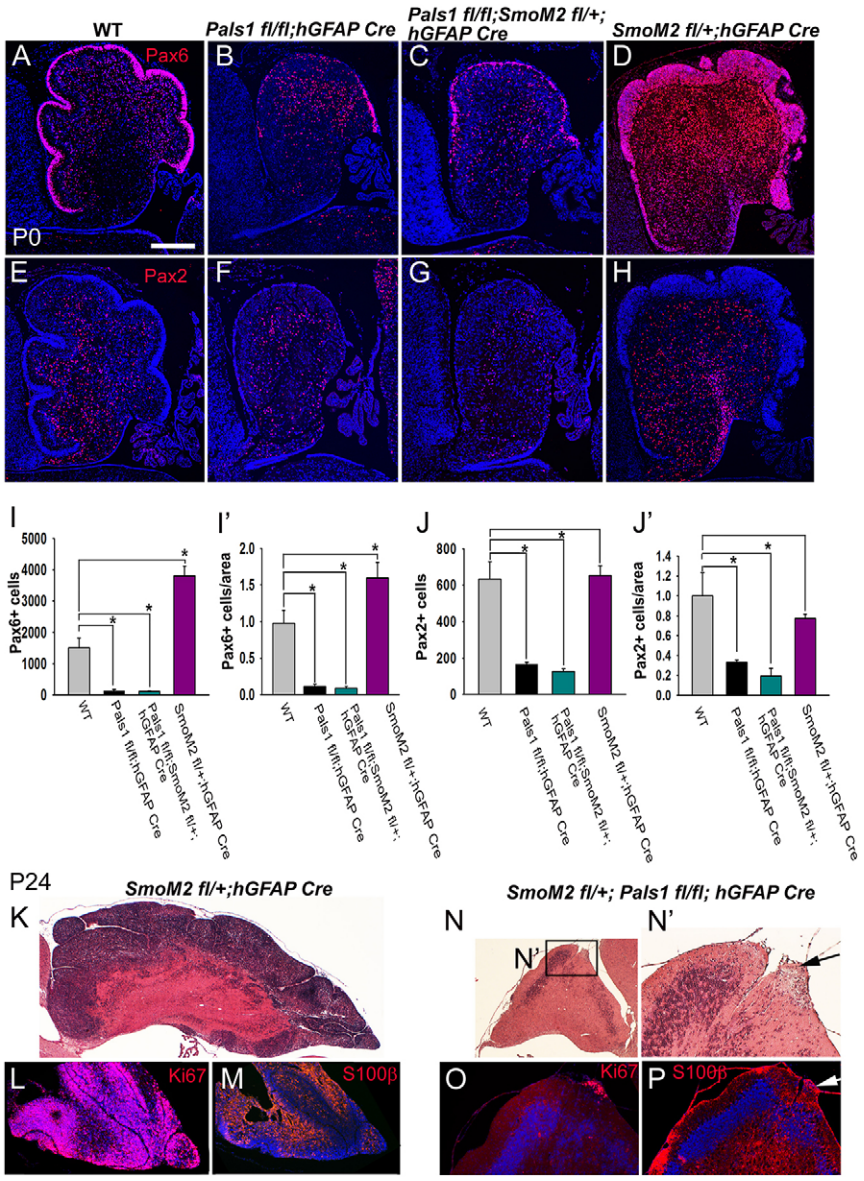


**Fig. 9. Pals1 deficiency blocks Smo-mediated, overactive Shh signaling.** (A-D,I,I′) The *SmoM2* allele induces overproduction of Pax6$^+$ cells and an expanded EGL (D) compared with WT ($n$=3, *$P$=0.046) at P0 (A). This is no longer observed in the double mutant with *Pals1* CKO ($n$=3, *$P$=0.0261) (C) or in *Pals1* CKO ($n$=3, *$P$=0.0094) (B). (E-H,J,J′) Pax2$^+$ interneurons are not increased in the *SmoM2* mutant (H) compared with WT (E) ($n$=3, $P$=0.1181). They are significantly decreased in the double mutant with *Pals1* CKO (G) ($n$=3, *$P$=0.0023), as in *Pals1* CKO (F) ($n$=3, *$P$=0.0192). (K-M) At P21, expanded dark and highly nuclear tissue indicates medulloblastoma in the *SmoM2* mutant. Many tumor cells are Ki67$^+$ (L), and S100β$^+$ and Ki67$^+$ cells do not appear to overlap (M). (N-P) In the double mutant, small clusters of eosinophilic cells, which are Ki67$^+$ (O) and S100β$^+$ (P), are found on the surface of the cerebellum (arrows). Scale bar: 100 µm in A-H.

epistatic function. One molecular mechanism by which Pals1 could regulate cell cycle progression is through interactions with other polarity complex proteins such as Par6 or aPKC. Aurora A and Polo-like kinase regulate asymmetric cell cycle progression in *Drosophila* by directly phosphorylating Par6 and Partner of numb (Pon), respectively (Wang et al., 2007; Wirtz-Peitz et al., 2008). Pals1 physically interacts with Par6 (Hurd et al., 2003), and our observation of disrupted apical localization of aPKC in the VZ of *Pals1* CKO supports the idea that Pals1 may control proliferation via these apical polarity proteins. Several lines of evidence have suggested that Par6 is engaged in cell proliferation, including that it shuttles between the cytoplasm/junction and nucleus, that a subtype of breast cancer shows genomic amplification of *Par6b*, and that forced Par6 expression leads to overproliferation in breast cancer cell lines (Nolan et al., 2008). Moreover, aPKC inhibits cell cycle exit and promotes cell division by directly phosphorylating p27 (Sabherwal et al., 2014). Taken together with these reports, our findings suggest that Pals1 may regulate the proliferation of cerebellar progenitor cells by directing the subcellular localization of these proteins.

Alternatively, Pals1 might serve as a permissive factor to promote the cell cycle progression of cerebellar progenitors. For instance, Pals1-mediated cell junction integrity between CGNPs and other progenitors might play a role in regulating cell proliferation. In the *Pals1* mutant, these cells might prematurely detach from the germinal zone and migrate out of the EGL, which could contribute to the loss of proliferative capability of CGNPs. The localization of other apical polarity complex proteins, including Crbs, has not been clearly determined in CGNPs owing to limitations in specificity. Crb at the apical junction is substantially reduced in the VZ of *Pals1* CKO, however, suggesting that its localization might also be disrupted in Pals1-deficient CGNPs. Previous studies have shown that homophilic interactions between extracellular domains of Crb proteins provide cell adhesion in the *Drosophila* wing (Letizia et al., 2013). Thus, the Pals1-Crb adhesion complex might play a crucial role in CGNP attachment in the EGL by enabling interactions between CGNPs or between CGNPs and pia meningeal cells until clonal expansion is completed. Future studies investigating Pals1-interacting proteins responsible for promoting cell cycle progression might yield novel regulatory pathways in cell cycle progression or adhesion.

Development (2016) 143, 133-146 doi:10.1242/dev.124180

### Pals1 function is required for BG genesis, migration and radial scaffold formation

Our analyses of *Pals1* mutants suggest a novel role for Pals1 in such aspects of BG development as production, migration and establishment of radial process morphology. Expression of Pals1 in developing, but not adult, BG, and the phenotype of short and stunted radial processes in the mutant, suggest that Pals1 has a cell-autonomous function in BG morphogenesis. Whether the specific aspect of BG layer formation at the PCL that requires Pals1 is loss of apical end-feet, soma translocation, proliferation or adhesion-mediated interaction with other cells, is not easily distinguishable in our *Pals1* deletion with *hGFAP-Cre* mice. Nonetheless, the dispersed distribution of BG in the absence of Pals1 appears to be the primary defect that prevents the cellular interactions required to form a tight epithelial-like layer in the PCL. Importantly, the compromised proliferation of BG and white matter progenitor cells, which provide another potential source of BG, may contribute to the disrupted BG layer formation because active proliferation is required to organize the expanding cerebellar cortex (Buffo and Rossi, 2013). It is also possible that Pals1 has a separate function directing the formation of BG unipolar radial processes and glia limitans at the pia surface, although the severely disrupted radial process phenotype in the mutant could be a secondary consequence of defects in BG production and migration. Further investigation with a more temporally controlled BG-specific *Pals1* deletion at different developmental time points will help to clarify whether Pals1 mainly controls BG migration or radial process formation.

One possible mechanism by which Pals1 loss may impair BG radial process formation is by disturbing the function or localization of known signaling molecules in pathways implicated in BG development, such as integrin, Notch and mTOR (Chen et al., 2013; Eiraku et al., 2005; Frick et al., 2012; Yue et al., 2005). Alternatively, Pals1-mediated adhesion of BG might be required to support radial process and layer formation by promoting interactions with other BG and PCs. Importantly, our study identifies Pals1 as a new molecular player in the generation, migration and, possibly, radial process formation of BG.

### Pals1 loss forces cell cycle exit despite hyperactive Shh signaling

Although *in vivo* mechanisms that stimulate CGNP cell cycle exit during development are not yet fully established, factors such as FGF, PKA and Wnt are known to drive differentiation *in vitro* and in tumor cells (Alvarez-Rodriguez et al., 2007; Fogarty et al., 2007; Lorenz et al., 2011; Masai et al., 2005; Wechsler-Reya and Scott, 1999). Recent studies have shown that Bcl6 overexpression (Tiberi et al., 2014) or direct FGF injection reduces proliferation of medulloblastoma cells in which Shh is hyperactivated (Emmenegger et al., 2013), supporting the idea that enhancing differentiation effectively prevents medulloblastoma progression *in vivo*.

Our data demonstrate that Pals1 deficiency can force cell cycle exit in CGNPs and in cells with malignant potential due to constitutively active Shh signaling. Although severe developmental defects in the *Pals1* mutant with *hGFAP-Cre* preclude us from unambiguously testing the direct effect of Pals1 loss in preventing uncontrolled proliferation of CGNPs, its crucial role in CGNP proliferation may support a cell-autonomous function with the potential to force the differentiation of cells with activated Shh signaling. Further examination of CGNP-specific Pals1 loss will be necessary to establish its role in malignant CGNP proliferation. It will also be important in future studies to determine the effect of removing Pals1 in mice with pre-existing medulloblastoma. Interestingly, a recent study shows that aPKC inhibitory peptides can block Gli1 phosphorylation and the subsequent propagation of tumor cells in basal cell carcinoma (Atwood et al., 2013). It is tempting to speculate that Pals1 and other apical polarity complex proteins might also play a downstream role in the Shh signaling pathway. Future experiments testing this possibility might provide a new direction for treating Shh-mediated medulloblastoma.

## MATERIALS AND METHODS

### Mice

Animals were handled in accordance with protocols approved by the IACUC of Temple University School of Medicine. *Pals1*$^{fl/fl}$ and *hGFAP-Cre* (Zhuo et al., 2001) or *Math1-Cre* (Matei et al., 2005) mice were bred for generation of CKO and genotyped by PCR as previously described (Kim et al., 2010). *SmoM2* mice (Jeong et al., 2004) were bred with *Pals1*$^{fl/fl}$ and *hGFAP-Cre* mice and genotyped by PCR as described previously (Zhuo et al., 2001).

### Histology and immunohistochemistry

Embryos at various developmental stages were decapitated and fixed in 4% paraformaldehyde (PFA) in PBS. For postnatal animals, brains were dissected out and fixed in 4% PFA in PBS. Fixed tissues were embedded in paraffin to prepare 6 µm parasagittal sections. Tissue sections were deparaffinized and rehydrated through an ethanol series and distilled water for Hematoxylin and Eosin (H&E) staining, immunofluorescence and immunohistochemistry. After 30 min of antigen retrieval with boiling citrate buffer, sections were stained with the antibodies described in the supplementary Materials and Methods. Alternatively, after incubation with the primary antibody, biotinylated anti-mouse or anti-rabbit secondary antibody was applied and incubated with peroxidase-conjugated avidin. Staining was visualized with a DAB (diaminobenzidine) substrate system (Sigma). Most analyses were performed on cerebellar midsagittal sections of comparable regions between WT and CKO (within 250 µm) for all stages. For data analyses, three animals and two non-consecutive sections/animal are used throughout the manuscript. Further details of phenotypic analyses can be found in the supplementary Materials and Methods.

### Western blot

Protein lysates were prepared from whole cerebellum at P0 for western blot analysis of reelin, Dab1 and phospho-Dab1 expression, with Gapdh as a standard, as described in the supplementary Materials and Methods.

### Brain size analyses

To measure cerebellum size, images of fixed brains were taken at the same magnification using an Axiophot microscope (Zeiss) to measure the width and length of the cerebellum. The images were analyzed and quantified in Photoshop (Adobe) or ImageJ (NIH), and statistical analysis was performed. To determine circumference, three histological images of midsagittal sections (vermis) per animal were measured using ImageJ. Three animals of each genotype were used to measure width, length and circumference.

### *In situ* hybridization

Fixed whole brains were washed with PBS and immersed in 30% sucrose for cryoprotection and embedded in OCT Compound (Tissue-Tek). Frozen samples were sectioned at 20 µm thickness. Paraffin samples were deparaffinized, rehydrated and dried at room temperature for 15-20 min. *In situ* hybridization was performed using antisense digoxigenin-labeled riboprobes by *in vitro* transcription of cDNAs: *Pals1* (coding region 867-1147 bp) *in situ* hybridization was carried out as previously described (Hui and Joyner, 1993).

### Bromodeoxyuridine (BrdU) administration and cell number quantification

BrdU (Sigma) dissolved in PBS was administered through intraperitoneal (IP) injection at 50 µg/g body weight for 30 min (acute) or 24 h (cell

Development (2016) 143, 133-146 doi:10.1242/dev.124180

cycle exit) before sacrifice. To analyze proliferation of EGL and VZ progenitors, the total number of $BrdU^+$ cells in the EGL or VZ in the image was counted manually using Photoshop and ImageJ at two midsagittal levels of each animal ($n$=3), after the acquisition of the images with an Axiophot microscope. Counting data are normalized with area for white matter (Sox9, Olig2, Pax6) or EGL (Pax6, BrdU, p27) or length for VZ (BrdU) and the relative value of the *Pals1* mutant is calculated as compared with WT. For cell cycle exit analyses, the same method was applied to count $Ki67^-$ and $BrdU^+$ and total $BrdU^+$ cells, and the fraction of $Ki67^-/BrdU^+$ cells among total $BrdU^+$ cells was calculated. For measuring the proportion of S-phase cells among total progenitor cells (BrdU index) after 30 min pulse labeling, we counted both $BrdU^+$ cells and $Ki67^+$ cells and calculated the fraction of $BrdU^+$ cells among total $Ki67^+$ cells for comparison with WT.

### Statistical analysis

The F-test was performed to determine whether the values were of equal or unequal variance before the *t*-test. Statistical significance was determined by Student's *t*-test for brain size analysis, cell counting of $BrdU^+$, $Pax6^+$, $BrdU^+/Pax6^+$, $Ki67^-/BrdU^+$, $Ki67^+$, $Olig2^+$, $Sox9^+$, $Pax2^+$ and $p27^+$ cells. $P<0.05$ was considered statistically significant.

### Real-time PCR

The Applied Biosystems StepOne and StepOnePlus Real-Time PCR system with LuminoCt SYBR Green qPCR ReadyMix (Sigma-Aldrich) were used. mRNA expression of three mutant and three WT embryos was analyzed. Expression levels of the genes of interest were normalized to actin (also known as *Actb*) in order to calculate the relative fold change compared with WT. Reaction mixtures included 10 µl 2× SYBR Green qPCR Ready Mix, 300 nM each primer and 1 µl cDNA template. The cDNA template was synthesized by reverse transcription of total RNA isolated from E17.5 cerebellum ($n$=3 for WT and CKO). Thermocycler parameters were 95°C for 10 min, followed by 40 cycles of 95°C for 15 s and 60°C for 1 min. All reactions were performed in triplicate. Primer sequences are provided in Table S3.

### Microarray

RNA was extracted from the cerebellum of four WT and four CKO embryos at E17.5 using the RNeasy Kit (Qiagen) and microarray experiments were conducted by the Microarray Core at the University of Texas, Houston. 300 ng total RNA was amplified and purified using the Illumina TotalPrep RNA Amplification Kit (Ambion, IL1791) following the manufacturer's instructions. Detailed methods are provided in the supplementary Materials and Methods. Microarray data have been deposited at GEO under accession number GSE75696.

#### Acknowledgements

We thank Drs Dwyer and Tessler for valuable comments on the manuscript; Dr Howell for providing the Dab1 antibody; and the Developmental Studies Hybridoma Bank at the University of Iowa for the mouse Pax6 antibody.

#### Competing interests

The authors declare no competing or financial interests.

#### Author contributions

S.K. and J.Y.P. conceived the project. J.Y.P. conducted most of the experiments. S.K., J.Y.P., L.J.H. and S.-H.C. prepared the manuscript. L.J.H. performed the initial analyses of CGNP-specific *Pals1* mutants and the *SmoM2* and *Pals1* double mutant. U.Y.M. performed the real-time PCR experiments. R.P. and K.T. contributed to the progenitor analyses. J.-S.L. and S.B.K. performed microarray data analyses.

#### Funding

This work was supported by grants from the National Institutes of Health to S.K. [RO1NS073112] and S.-H.C. [RO1EY020578] and Shriners Hospitals Pediatric Research Center startup funds. Deposited in PMC for release after 12 months.

#### Supplementary information

Supplementary information available online at
http://dev.biologists.org/lookup/suppl/doi:10.1242/dev.124180/-/DC1

#### References

**Alvarez-Rodriguez, R., Barzi, M., Berenguer, J. and Pons, S.** (2007). Bone morphogenetic protein 2 opposes Shh-mediated proliferation in cerebellar granule cells through a TIEG-1-based regulation of Nmyc. *J. Biol. Chem.* **282**, 37170-37180.

**Assémat, E., Bazellières, E., Pallesi-Pocachard, E., Le Bivic, A. and Massey-Harroche, D.** (2008). Polarity complex proteins. *Biochim. Biophys. Acta* **1778**, 614-630.

**Atwood, S. X., Li, M., Lee, A., Tang, J. Y. and Oro, A. E.** (2013). GLI activation by atypical protein kinase C iota/lambda regulates the growth of basal cell carcinomas. *Nature* **494**, 484-488.

**Buffo, A. and Rossi, F.** (2013). Origin, lineage and function of cerebellar glia. *Prog. Neurobiol.* **109**, 42-63.

**Bultje, R. S., Castaneda-Castellanos, D. R., Jan, L. Y., Jan, Y.-N., Kriegstein, A. R. and Shi, S.-H.** (2009). Mammalian Par3 regulates progenitor cell asymmetric division via notch signaling in the developing neocortex. *Neuron* **63**, 189-202.

**Chen, S., Chen, J., Shi, H., Wei, M., Castaneda-Castellanos, D. R., Bultje, R. S., Pei, X., Kriegstein, A. R., Zhang, M. and Shi, S.-H.** (2013). Regulation of microtubule stability and organization by Mammalian par3 in specifying neuronal polarity. *Dev. Cell* **24**, 26-40.

**Chizhikov, V. V., Lindgren, A. G., Mishima, Y., Roberts, R. W., Aldinger, K. A., Miesegaes, G. R., Currle, D. S., Monuki, E. S. and Millen, K. J.** (2010). Lmx1a regulates fates and location of cells originating from the cerebellar rhombic lip and telencephalic cortical hem. *Proc. Natl. Acad. Sci. USA* **107**, 10725-10730.

**Cho, S.-H., Kim, J. Y., Simons, D. L., Song, J. Y., Le, J. H., Swindell, E. C., Jamrich, M., Wu, S. M. and Kim, S.** (2012). Genetic ablation of Pals1 in retinal progenitor cells models the retinal pathology of Leber congenital amaurosis. *Hum. Mol. Genet.* **21**, 2663-2676.

**Costa, M. R., Wen, G., Lepier, A., Schroeder, T. and Gotz, M.** (2008). Par-complex proteins promote proliferative progenitor divisions in the developing mouse cerebral cortex. *Development* **135**, 11-22.

**Eiraku, M., Tohgo, A., Ono, K., Kaneko, M., Fujishima, K., Hirano, T. and Kengaku, M.** (2005). DNER acts as a neuron-specific Notch ligand during Bergmann glial development. *Nat. Neurosci.* **8**, 873-880.

**Emmenegger, B. A., Hwang, E. I., Moore, C., Markant, S. L., Brun, S. N., Dutton, J. W., Read, T.-A., Fogarty, M. P., Singh, A. R., Durden, D. L. et al.** (2013). Distinct roles for fibroblast growth factor signaling in cerebellar development and medulloblastoma. *Oncogene* **32**, 4181-4188.

**Espinosa, J. S. and Luo, L.** (2008). Timing neurogenesis and differentiation: insights from quantitative clonal analyses of cerebellar granule cells. *J. Neurosci.* **28**, 2301-2312.

**Famulski, J. K., Trivedi, N., Howell, D., Yang, Y., Tong, Y., Gilbertson, R. and Solecki, D. J.** (2010). Siah regulation of Pard3A controls neuronal cell adhesion during germinal zone exit. *Science* **330**, 1834-1838.

**Fogarty, M. P., Emmenegger, B. A., Grasfeder, L. L., Oliver, T. G. and Wechsler-Reya, R. J.** (2007). Fibroblast growth factor blocks Sonic hedgehog signaling in neuronal precursors and tumor cells. *Proc. Natl. Acad. Sci. USA* **104**, 2973-2978.

**Frick, A., Grammel, D., Schmidt, F., Pöschl, J., Priller, M., Pagella, P., von Bueren, A. O., Peraud, A., Tonn, J.-C., Herms, J. et al.** (2012). Proper cerebellar development requires expression of beta1-integrin in Bergmann glia, but not in granule neurons. *Glia* **60**, 820-832.

**Hui, C. C. and Joyner, A. L.** (1993). A mouse model of greig cephalopolysyndactyly syndrome: the extra-toesJ mutation contains an intragenic deletion of the Gli3 gene. *Nat. Genet.* **3**, 241-246.

**Hurd, T. W., Gao, L., Roh, M. H., Macara, I. G. and Margolis, B.** (2003). Direct interaction of two polarity complexes implicated in epithelial tight junction assembly. *Nat. Cell Biol.* **5**, 137-142.

**Ishiuchi, T., Misaki, K., Yonemura, S., Takeichi, M. and Tanoue, T.** (2009). Mammalian Fat and Dachsous cadherins regulate apical membrane organization in the embryonic cerebral cortex. *J. Cell Biol.* **185**, 959-967.

**Jeong, J., Mao, J., Tenzen, T., Kottmann, A. H. and McMahon, A. P.** (2004). Hedgehog signaling in the neural crest cells regulates the patterning and growth of facial primordia. *Genes Dev.* **18**, 937-951.

**Julian, E., Hallahan, A. R. and Wainwright, B. J.** (2010). RBP-J is not required for granule neuron progenitor development and medulloblastoma initiated by Hedgehog pathway activation in the external germinal layer. *Neural Dev.* **5**, 27.

**Kim, S., Lehtinen, M. K., Sessa, A., Zappaterra, M. W., Cho, S.-H., Gonzalez, D., Boggan, B., Austin, C. A., Wijnholds, J., Gambello, M. J. et al.** (2010). The apical complex couples cell fate and cell survival to cerebral cortical development. *Neuron* **66**, 69-84.

**Letizia, A., Ricardo, S., Moussian, B., Martin, N. and Llimargas, M.** (2013). A functional role of the extracellular domain of Crumbs in cell architecture and apicobasal polarity. *J. Cell Sci.* **126**, 2157-2163.

**Li, K., Leung, A. W., Guo, Q., Yang, W. and Li, J. Y.** (2014). Shp2-dependent ERK signaling is essential for induction of Bergmann glia and foliation of the cerebellum. *J. Neurosci.* **34**, 922-931.

**Lorenz, A., Deutschmann, M., Ahlfeld, J., Prix, C., Koch, A., Smits, R., Fodde, R., Kretzschmar, H. A. and Schuller, U.** (2011). Severe alterations of cerebellar

cortical development after constitutive activation of Wnt signaling in granule neuron precursors. *Mol. Cell. Biol.* **31**, 3326-3338.
**Machold, R. and Fishell, G.** (2005). Math1 is expressed in temporally discrete pools of cerebellar rhombic-lip neural progenitors. *Neuron* **48**, 17-24.
**Maricich, S. M. and Herrup, K.** (1999). The Pax-2 expression defines a subset of GABAergic interneurons and their precursors in the developing murine cerebellum. *J. Neurobiol.* **41**, 281-294.
**Masai, I., Yamaguchi, M., Tonou-Fujimori, N., Komori, A. and Okamoto, H.** (2005). The hedgehog-PKA pathway regulates two distinct steps of the differentiation of retinal ganglion cells: the cell-cycle exit of retinoblasts and their neuronal maturation. *Development* **132**, 1539-1553.
**Mason, C. A., Edmondson, J. C. and Hatten, M. E.** (1988). The extending astroglial process: development of glial cell shape, the growing tip, and interactions with neurons. *J. Neurosci.* **8**, 3124-3134.
**Matei, V., Pauley, S., Kaing, S., Rowitch, D., Beisel, K. W., Morris, K., Feng, F., Jones, K., Lee, J. and Fritzsch, B.** (2005). Smaller inner ear sensory epithelia in Neurog1 null mice are related to earlier hair cell cycle exit. *Dev. Dyn.* **234**, 633-650.
**Millen, K. J. and Gleeson, J. G.** (2008). Cerebellar development and disease. *Curr. Opin. Neurobiol.* **18**, 12-19.
**Noatynska, A., Tavernier, N., Gotta, M. and Pintard, L.** (2013). Coordinating cell polarity and cell cycle progression: what can we learn from flies and worms? *Open Biol.* **3**, 130083.
**Nolan, M. E., Aranda, V., Lee, S., Lakshmi, B., Basu, S., Allred, D. C. and Muthuswamy, S. K.** (2008). The polarity protein Par6 induces cell proliferation and is overexpressed in breast cancer. *Cancer Res.* **68**, 8201-8209.
**Page, B. D., Guedes, S., Waring, D. and Priess, J. R.** (2001). The C. elegans E2F- and DP-related proteins are required for embryonic asymmetry and negatively regulate Ras/MAPK signaling. *Mol. Cell* **7**, 451-460.
**Parmigiani, E., Leto, K., Rolando, C., Figueres-Onate, M., Lopez-Mascaraque, L., Buffo, A. and Rossi, F.** (2015). Heterogeneity and bipotency of astroglial-like cerebellar progenitors along the interneuron and glial lineages. *J. Neurosci.* **35**, 7388-7402.
**Pieczynski, J. and Margolis, B.** (2011). Protein complexes that control renal epithelial polarity. *Am. J. Physiol. Renal Physiol.* **300**, F589-F601.
**Rabilotta, A., Desrosiers, M. and Labbé, J.-C.** (2015). CDK-1 and two B-type cyclins promote PAR-6 stabilization during polarization of the early C. elegans embryo. *PLoS ONE* **10**, e0117656.
**Roh, M. H., Fan, S., Liu, C.-J. and Margolis, B.** (2003). The Crumbs3-Pals1 complex participates in the establishment of polarity in mammalian epithelial cells. *J. Cell Sci.* **116**, 2895-2906.
**Roussel, M. F. and Hatten, M. E.** (2011). Cerebellum: development and medulloblastoma. *Curr. Top. Dev. Biol.* **94**, 235-282.
**Roussel, M. F. and Robinson, G. W.** (2013). Role of MYC in medulloblastoma. *Cold Spring Harb. Perspect. Med.* **3**, a014308.
**Sabherwal, N., Thuret, R., Lea, R., Stanley, P. and Papalopulu, N.** (2014). aPKC phosphorylates p27Xic1, providing a mechanistic link between apicobasal polarity and cell-cycle control. *Dev. Cell* **31**, 559-571.
**Shi, S.-H., Jan, L.-Y. and Jan, Y.-N.** (2003). Hippocampal neuronal polarity specified by spatially localized mPar3/mPar6 and PI 3-kinase activity. *Cell* **112**, 63-75.
**Solecki, D. J., Govek, E.-E. and Hatten, M. E.** (2006). mPar6 alpha controls neuronal migration. *J. Neurosci.* **26**, 10624-10625.
**St Johnston, D. and Ahringer, J.** (2010). Cell polarity in eggs and epithelia: parallels and diversity. *Cell* **141**, 757-774.
**Sudarov, A. and Joyner, A. L.** (2007). Cerebellum morphogenesis: the foliation pattern is orchestrated by multi-cellular anchoring centers. *Neural Dev.* **2**, 26.
**Sudarov, A., Turnbull, R. K., Kim, E. J., Lebel-Potter, M., Guillemot, F. and Joyner, A. L.** (2011). Ascl1 genetics reveals insights into cerebellum local circuit assembly. *J. Neurosci.* **31**, 11055-11069.
**Tanabe, K., Kani, S., Shimizu, T., Bae, Y.-K., Abe, T. and Hibi, M.** (2010). Atypical protein kinase C regulates primary dendrite specification of cerebellar Purkinje cells by localizing Golgi apparatus. *J. Neurosci.* **30**, 16983-16992.
**Taylor, M. D., Northcott, P. A., Korshunov, A., Remke, M., Cho, Y.-J., Clifford, S. C., Eberhart, C. G., Parsons, D. W., Rutkowski, S., Gajjar, A. et al.** (2012). Molecular subgroups of medulloblastoma: the current consensus. *Acta Neuropathol.* **123**, 465-472.
**Tepass, U.** (2012). The apical polarity protein network in Drosophila epithelial cells: regulation of polarity, junctions, morphogenesis, cell growth, and survival. *Annu. Rev. Cell Dev. Biol.* **28**, 655-685.
**Tiberi, L., Bonnefont, J., van den Ameele, J., Le Bon, S.-D., Herpoel, A., Bilheu, A., Baron, B. W. and Vanderhaeghen, P.** (2014). A BCL6/BCOR/SIRT1 complex triggers neurogenesis and suppresses medulloblastoma by repressing Sonic Hedgehog signaling. *Cancer Cell* **26**, 797-812.
**Wang, H., Ouyang, Y., Somers, W. G., Chia, W. and Lu, B.** (2007). Polo inhibits progenitor self-renewal and regulates Numb asymmetry by phosphorylating Pon. *Nature* **449**, 96-100.
**Wechsler-Reya, R. J. and Scott, M. P.** (1999). Control of neuronal precursor proliferation in the cerebellum by Sonic Hedgehog. *Neuron* **22**, 103-114.
**Wingate, R. J. and Hatten, M. E.** (1999). The role of the rhombic lip in avian cerebellum development. *Development* **126**, 4395-4404.
**Wirtz-Peitz, F., Nishimura, T. and Knoblich, J. A.** (2008). Linking cell cycle to asymmetric division: Aurora-A phosphorylates the Par complex to regulate Numb localization. *Cell* **135**, 161-173.
**Yue, Q., Groszer, M., Gil, J. S., Berk, A. J., Messing, A., Wu, H. and Liu, X.** (2005). PTEN deletion in Bergmann glia leads to premature differentiation and affects laminar organization. *Development* **132**, 3281-3291.
**Zervas, M., Blaess, S. and Joyner, A. L.** (2005). Classical embryological studies and modern genetic analysis of midbrain and cerebellum development. *Curr. Top. Dev. Biol.* **69**, 101-138.
**Zhuo, L., Theis, M., Alvarez-Maya, I., Brenner, M., Willecke, K. and Messing, A.** (2001). hGFAP-cre transgenic mice for manipulation of glial and neuronal function in vivo. *Genesis* **31**, 85-94.

## SUPPLEMENTARY INFORMATION

**Title:** Apical complex protein Pals1 is required to maintain cerebellar progenitor cells in a proliferative state

**Running title: Pals1 role in cerebellum development**

Jun Young Park[1], Lucinda J. Hughes[1,2], Uk Yeol Moon[1], Raehee Park[1], Sang Bae Kim, Khoi Tran[1,], Ju-Seug Lee[3], Seo-Hee Cho[1] and Seonhee Kim[1*]
[1]*Shriners Hospitals Pediatric Research Center, Department of Anatomy and Cell Biology, Temple University School of Medicine, Philadelphia, PA, 19140, USAGraduate program of Biomedical Sciences, Temple University School of Medicine, Philadelphia, PA, 19140, USA*
[3]*Department of Systems biology, MD Anderson cancer center, University of Texas, Houston, TX, 77030, USA*

## SUPPLEMENTARY MATERIALS AND METHODS

### Phenotype analyses

To ensure sections were in the midsagittal plane, we limited collection to about 42 sections (6μm each) from each cerebellum hemisphere originally cut along the midline of the vermis. A few images (Fig. 3C, D and Fig. 8K-N) are from sections outside of the range of the midsagittal plane as defined by the above criteria. In these cases, comparable sections were carefully selected by examining surrounding brainstem structures such as midbrain and pons. Most of enlarged areas are indicated in the lower magnification figures except Figure 3 E, F: between lobe 3 and 4, G, H: lobe 10, K, L lobes 3-5, M, N: lobe 10 and Fig. 5 O, P lobes: 2 and 3.

### Immunostaining

Primary antibodies were BrdU (1:50; Becton Dickinson Immunocytometry Systems, 347580), phospho-histone H3 (PH3) (1:250; Millipore, 06570), Pals1 (1:250, Upstate, 07-708), PKCλ (1:250; BD Biosciences, 610193), Reelin (1:250; Millipore, MAB5364), BLBP (1:250; Millipore, ABN14), Dab1 (gift from Dr. Howell), S100β (1:250; Novus Biologicals, NB110-57478), Pax2

(1:250; Covance, PRB-276P), p27 (1:250; BD Biosciences, 610241), Pax6 (1:250; Covance, RBP-278P), Pax6 (1:250; Developmental Studies Hybridoma Bank), Calbindin (1:250; Sigma, C9848), GFAP (1:250; Thermo Scientific, RB-087), Par3 (1:250; Millipore, 07330), Zo1 (1:250; BD Biosciences, 610967), N-Cadherin (1:250; BD Biosciences, 610920), Cleaved Caspase-3 (1:250; Cell Signaling, #9661), Pan Crb (1:250; produced in the lab), Tuj1 (1:250; Millipore, MAB1637), phospho-vimentin (4A4) (1:250; MBL, D076-3), Ki67 (1:1000; Leica biosystem, KCL-Ki67P), Parvalbumin (1:250; Millipore, MAB1572), and NeuN (1:250; Millipore, MAB377). Species-specific Alexa Fluor 488 (1:500; Invitrogen) and Cy3 (1:500; Jackson Immunochemical) secondary antibodies were used for fluorescence detection, and nuclear DNA was counterstained with Hoechst 22358 (1:1000; Invitrogen).

**Western Blot analysis**

Whole cerebellums were dissected at postnatal day 0 to prepare protein lysates, and meninges were removed from the tissue. Protein lysates were homogenized in ice-chilled cell lysis buffer (20mM Tris-HCL (pH 7.5), 150mM NaCl, 1mM $Na_2EDTA$, 1mM EGTA, 1% Triton, 2.5 mM sodium pyrophosphate, 1mM beta-glycerophosphate, 1mM $Na_3VO_4$, and 1μg/ml leupeptin) containing 1% Protease Inhibitor Cocktail P8340 (Sigma). Using an SDS-PAGE gel, protein lysates were separated and transferred to a polyvinylidene difluoride membrane. The membrane was blocked with 5% nonfat dry milk, and primary antibodies were applied at 4°C overnight. The primary antibodies included Reelin (1:500; Millipore), Dab1 (1:500; Cell Signaling), phospho-Dab1 (1:500; Cell Signaling) and GAPDH (1:500; Cell Signaling). Expression signals were detected by chemiluminescence (ECL Kit; GE Healthcare).

**Microarray**

First strand cDNA was synthesized by incubating RNA with oligo(dT) primer and reverse transcriptase mix at 42 $^{o}$C for 2 hours. RNase H and DNA polymerase master mix were immediately added to the reaction mix following reverse transcription and were incubated for 2 hours at 16 $^{o}$C to synthesize second strand cDNA. *In vitro* transcription was performed and biotinylated cRNA was synthesized. An aliquot of 750 ng of amplified cRNA was loaded onto Illumina Sentrix Beadchip Array Mouse Ref8.v2 arrays, hybridized at 58$^{o}$C in an Illumina Hybridization Oven (Illumina, Cat# 198361) for 17 hours, washed, and incubated with straptavidin-Cy3 to detect biotin-labeled cRNA on the arrays. Arrays were dried and scanned with BeadArray Reader (Illumina, CA). Microarray data were normalized using the quantile normalization method in the Linear Models for Microarray Data (LIMMA) package in the R language (http://www.r-project.org). BRB-ArrayTools was used for statistical analysis of gene expression data and the t-test was applied to identify which genes differed between the two groups (Cancer Inform. 2007; 3: 11–17). Cluster analysis was performed using the Cluster software and Heatmap was generated by Treeview (Proc Natl Acad Sci U S A. 1998 Dec 8;95(25):14863-8). Network analysis was performed by Ingenuity Pathway Analysis software 9 (http://www.ingenuity.com). Ingenuity Pathways Analysis computes a score for each network according to the fit of that network to the user-defined set of Focus Genes. The p-value is the probability of finding f or more Focus Genes in a set of n genes randomly selected from the Global Molecular Network. The p-score is defined as: P-score = -log10 (p-value)

## SUPPLEMENTARY FIGURES

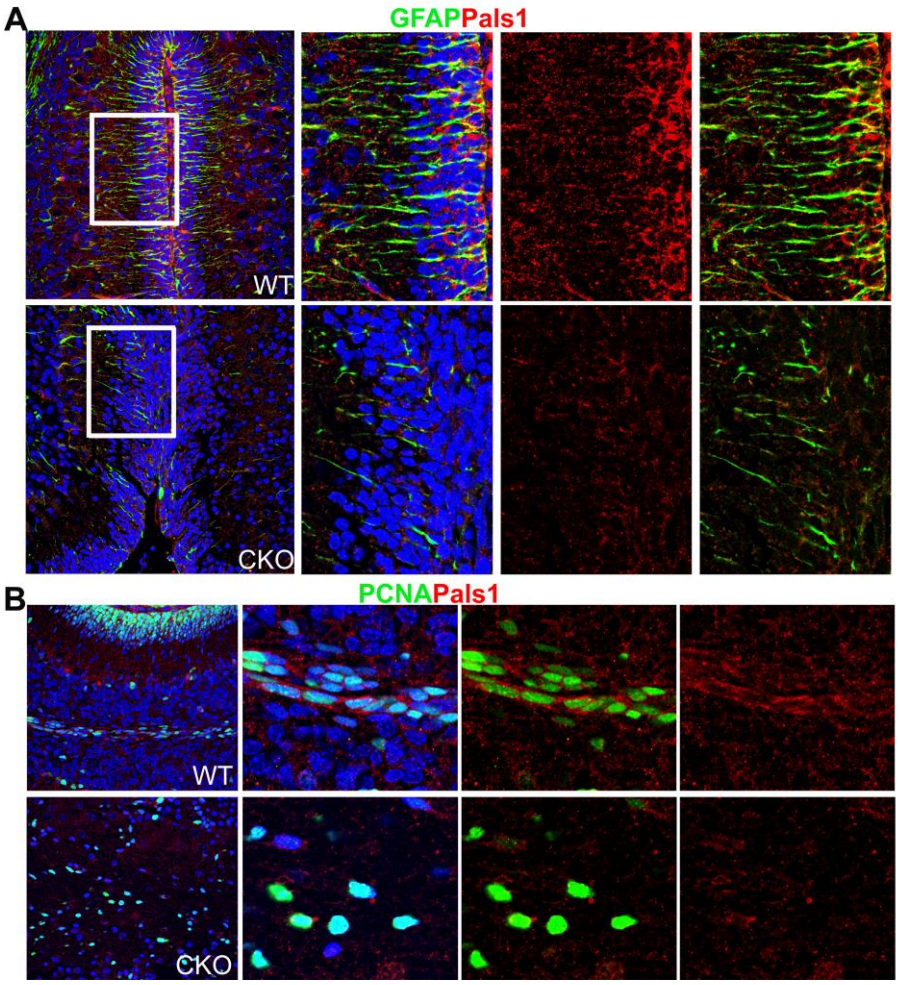


**Fig. S1 Pals1 expression in BG fibers and progenitors in the white matter is diminished in *Pals1* CKO**

**(A)** At P8, Pals1 immunostaining overlaps with GFAP + BG processes but expression of Pals1 is substantially reduced in EGL and BG processes in the *Pals1* CKO. **(B)** PCNA+ proliferating cells in the white matter show Pals1 expression, which is decreased in the *Pals1* CKO.

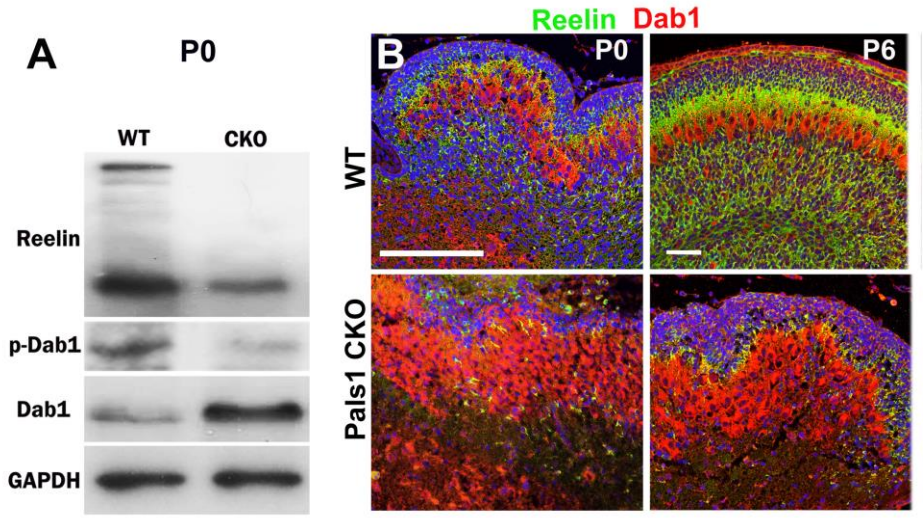


**Fig. S2 Reelin/ Dab1 signaling is impaired in the *Pals1* CKO cerebellum**

(**A**) Western blot analysis of P0 lysate shows a significant reduction of Reelin and p-Dab1, but an increase of Dab1, indicative of ineffective Reelin signaling, in the *Pals1* CKO. (**B**) In accordance with Western blot analysis, immunostaining of the *Pals1* CKO shows reduced Reelin and increased Dab1 at both P0 and P6.

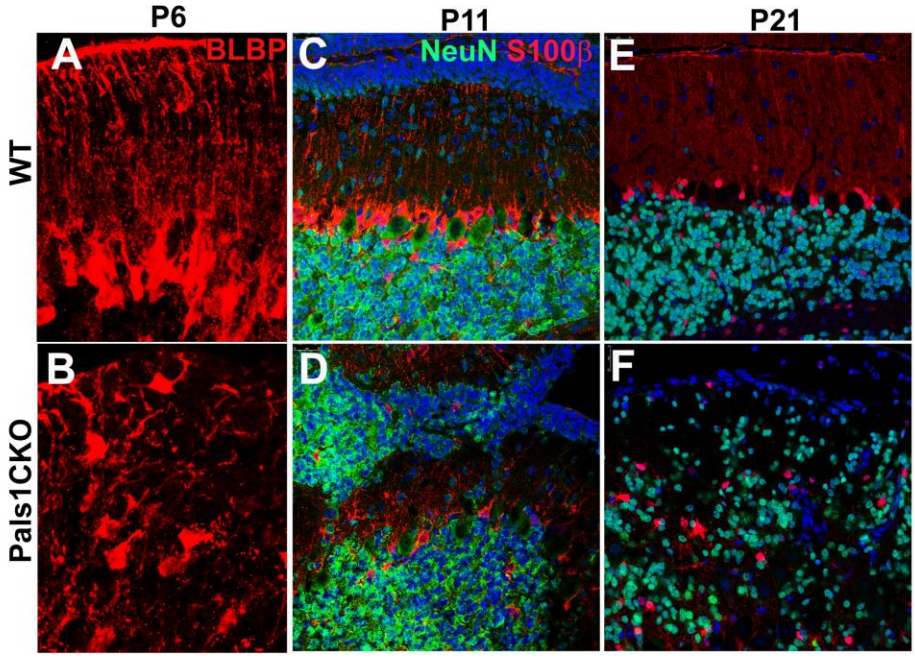


**Fig. S3 Defective inward migration of CGNs in the *Pals1* CKO**

**(A, B)** At P6, BLBP+ glia cells are scattered in the molecular layer with stunted morphology in the *Pals1* mutant while BLBP+ glia cells in the WT are concentrated in PCL and radial glia fibers reach the pia surface. **(C, D)** At P11, clusters of NeuN positive CGNs remain just beneath the pia in the *Pals1* mutant, where NeuN negative undifferentiated CGNPs reside in the WT. S100β positive glia cells are scattered throughout the molecular layer in the mutants. **(E, F)** At P21, NeuN+ neurons failed to form layers and are randomly distributed in the cerebellum.

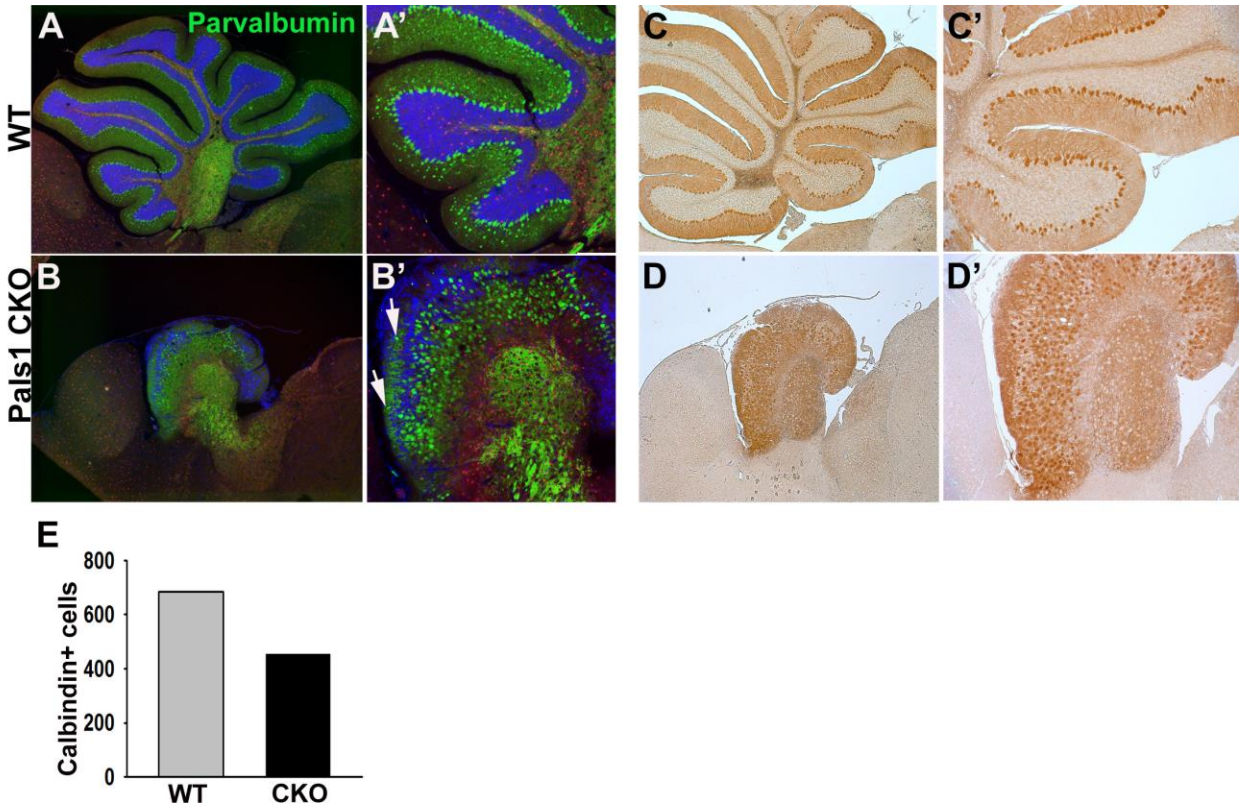


**Fig. S4 The generation of mature interneurons is impaired in the *Pals1* CKO**

**(A, A', B, B'**) Parvalbumin immunostaining detects interneurons in the molecular layer and PCs, which have larger cell bodies, in the WT **(A, A')**. Parvalbumin positive interneurons are rare in the poorly developed molecular layer of *Pals1* CKO at P21 (arrows, **B'**). In contrast, Parvalbumin positive large PC cells remained abundant in the *Pals1* CKO, which is consistent with immunostaining with Calbindin **(C, C', D, D')**. However, the number of Calbindin+ cells in the CKO is reduced compared to WT **(E)**.

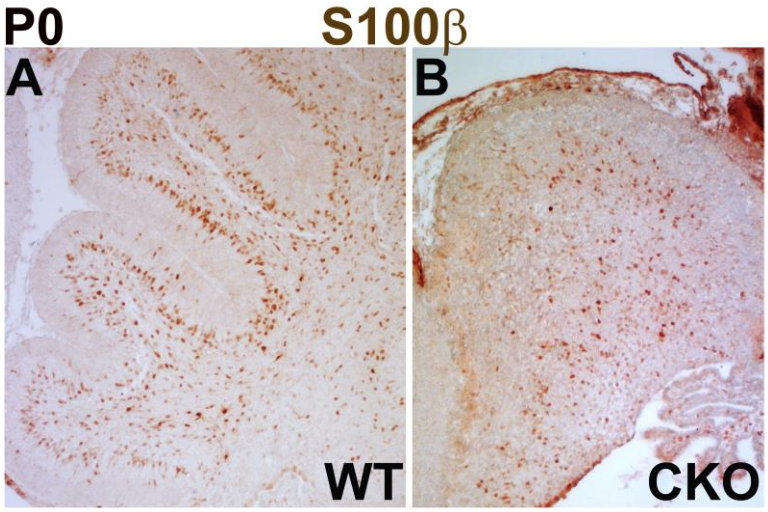


**Fig. S5 Production and distribution of glia cells are defective in the *Pals1* CKO**

**(A, B)** S100β immunostaining reveals a significant reduction of glia cells with dispersed distribution in the *Pals1* CKO compared to WT at P0.

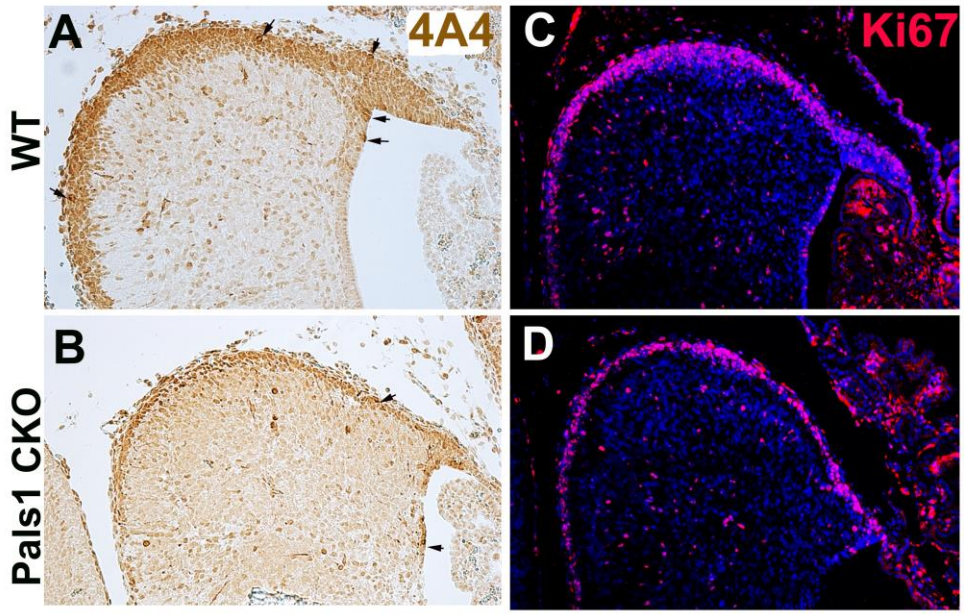


**Fig. S6 Reduction of proliferating CGN cells at the EGL in the *Pals1* CKO**

**(A, B)** Phospho-Vimentin (4A4) immunostaining intensely visualizes the membrane of mitotic cells (arrows) and a population of proliferating cells at the EGL of WT; the amount of 4A4 positive cells is strikingly reduced in the *Pals1* CKO. (**C**-**D**) Ki67 immunopositive proliferating cells are decreased in the EGL, URL and VZ of the *Pals1* CKO compared to WT.

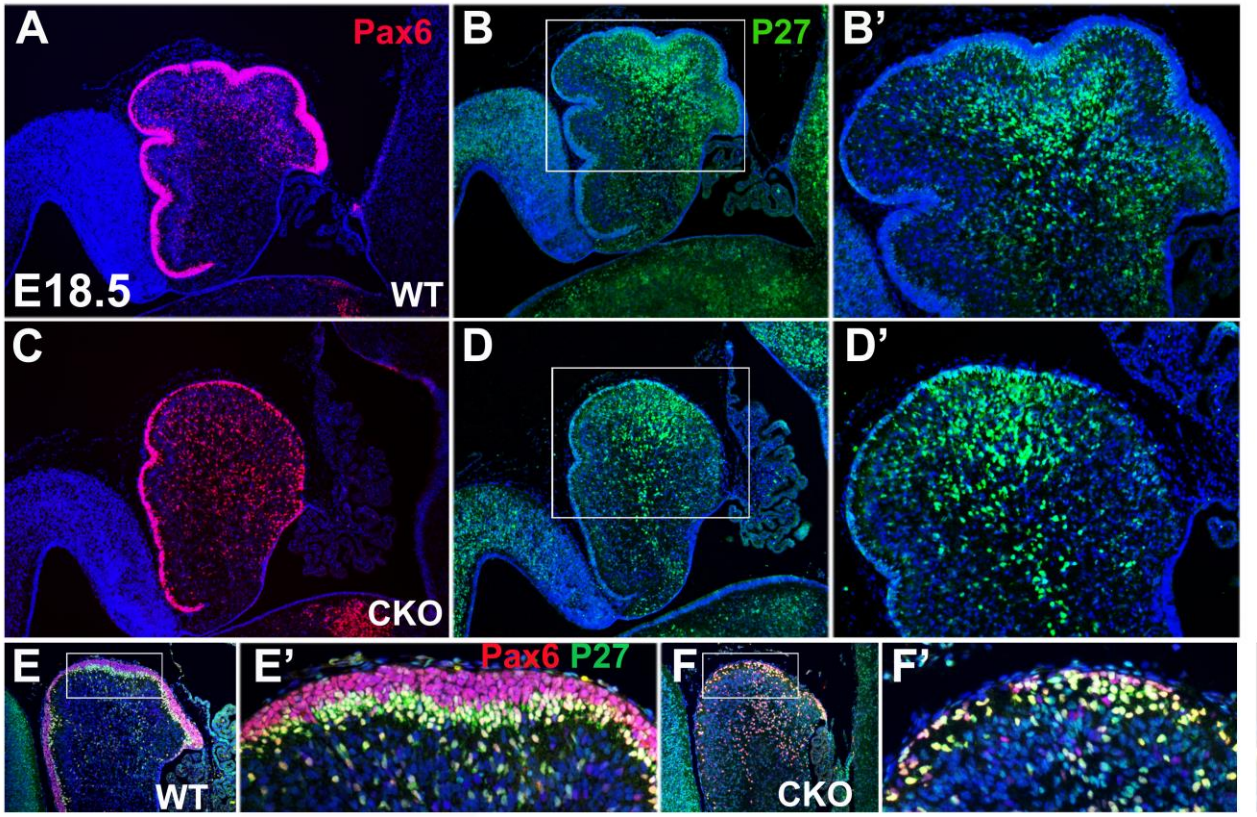


**Fig. S7 Pals1 deficiency causes premature differentiation of CGNPs**

**(A, C)** More Pax6+ cells are distributed deeper in the cerebellar plate and fewer Pax6+ cells remained in the EGL of the CKO compared to WT. **(B, B', D, D')** Cell cycle inhibitor p27 Kip1 (p27) expression extends to the top of cerebellar plate beneath the pia in the mutant where proliferating (p27–) cells are found in WT at E18.5 (**B'** and **D'** are enlarged images of **B, D**, respectively). **(E, E', F, F')** At E17.5, reduced numbers of Pax6 expressing cells are in the EGL of *Pals1* CKO compared to WT, and p27 expressing cells are also found proximal to the pia in the *Pals1* CKO. (**E'** and **F'** are enlarged images of boxed area of **E, F**, respectively.)

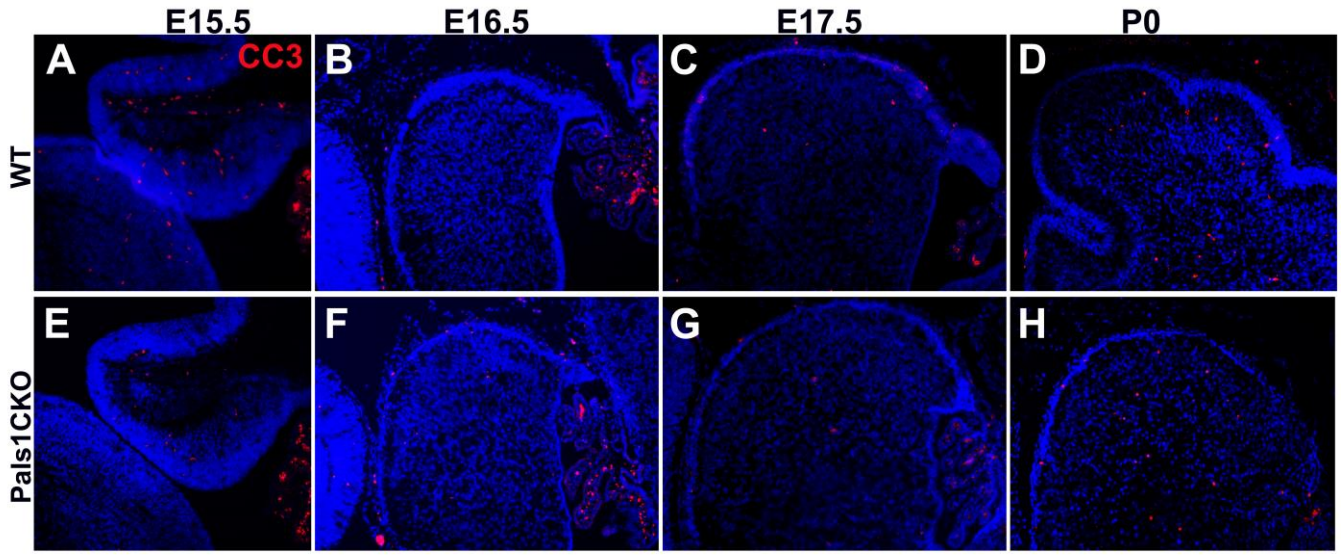


**Fig. S8 Apoptotic cell death is not increased in the *Pals1* CKO**

**(A-H)** Population of dying cells identified by CC3 immunostaining is not obviously greater in the *Pals1* CKO than in WT during embryogenesis (E15.5, E16.5 and E17.5) or in neonates.

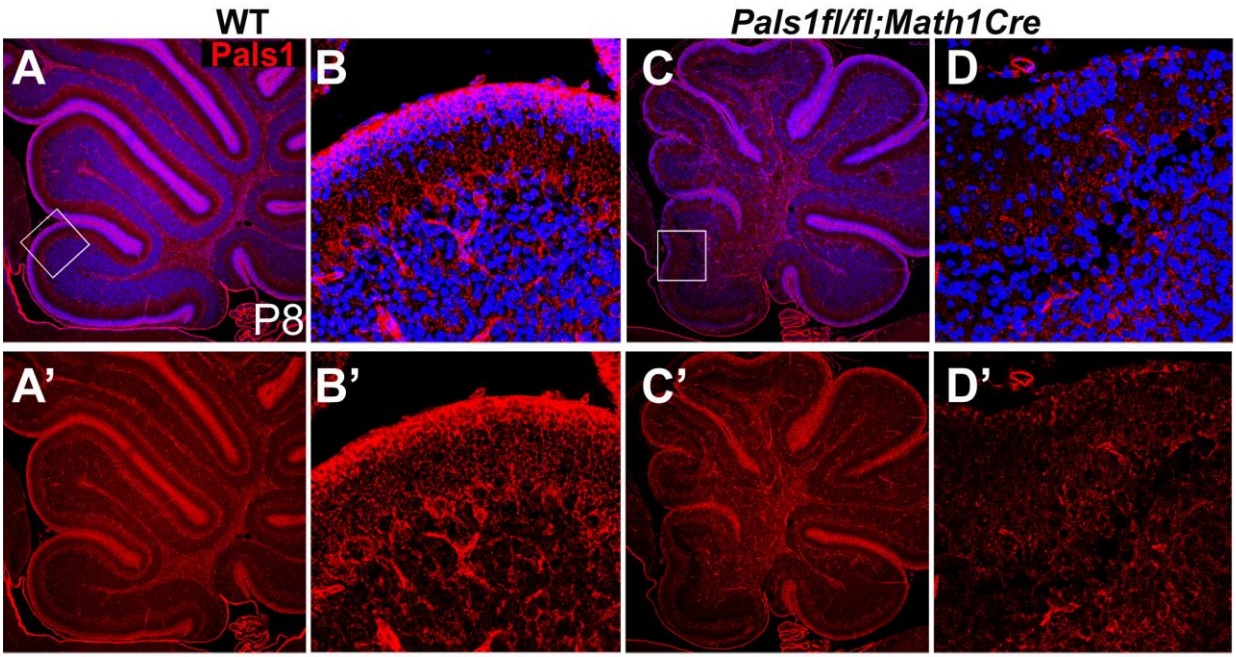


**Fig. S9** ***Math1 Cre*** **mediated** ***Pals1*** **deletion reduces Pals1 expression and cerebellar size**

**(A-D')** At P8, Pals1 is highly expressed in the EGL, PC layer and white matter. The removal of Pals1 by *Math1 Cre* is most effective in lobe 1 and the anterior part of lobe 2, while detectable Pals1 immunosignal remains in the EGL of other lobes.

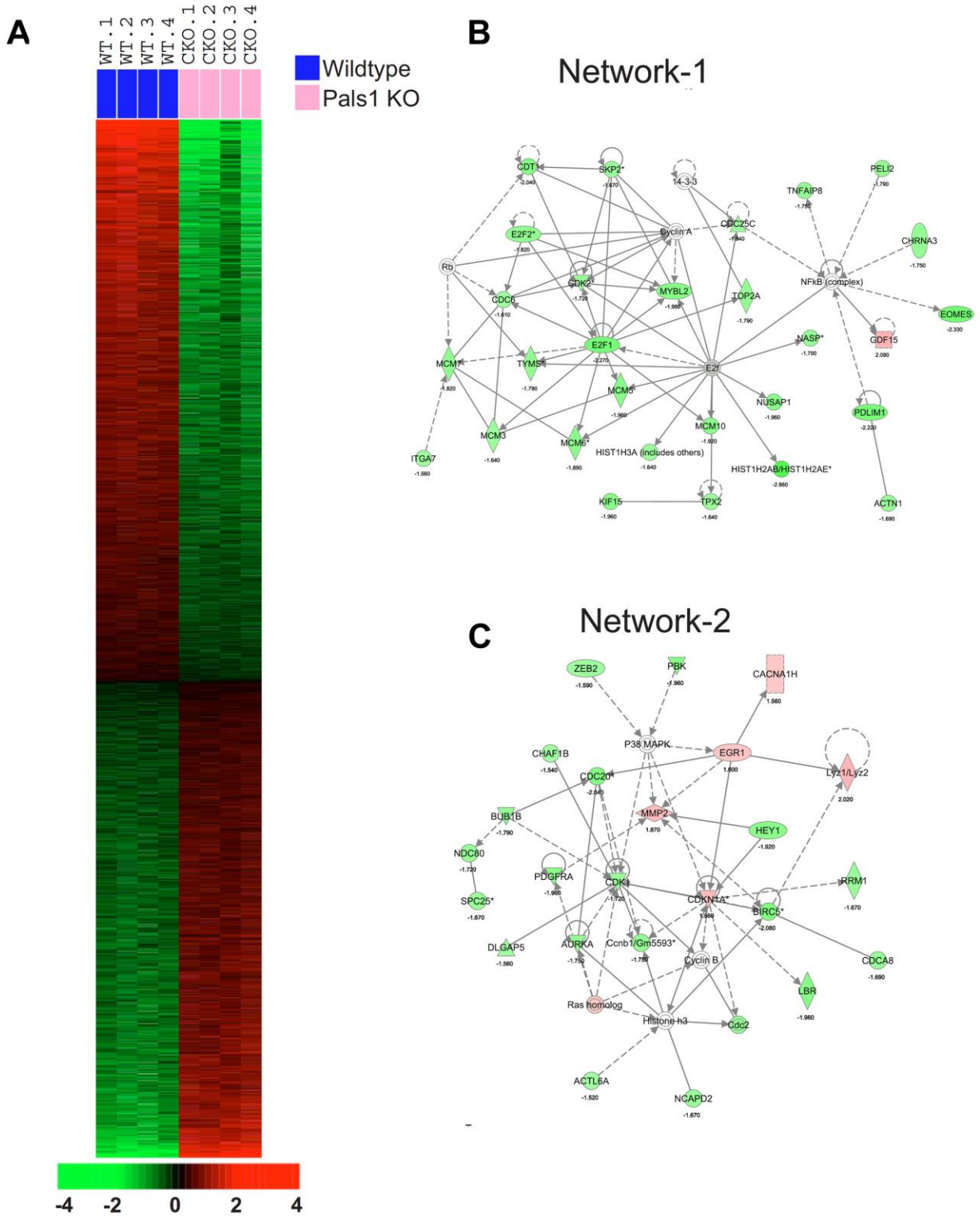

**Fig. S10 Ingenuity pathway analysis**

**(A)** Genes with significantly altered expression in *Pals1* CKO were selected by comparing two groups of cerebellum (4 each) at E17.5 . Expression of 762 genes are significantly altered in *Pals1* CKO compared to WT. Data is presented in a matrix format in which each row represents a gene and each column represents a cerebellum sample. The coloring in the cells reflects relatively high (red) and low (green) expression levels as indicated by the scale bar at the bottom (Log2 –transformed scale). **(B)** The two highest ranked networks affected by Pals1 loss are Cell Cycle, DNA Replication, Recombination, Repair, Cellular Assembly and Organization and (Network-1) and Cell Cycle, Cancer, Respiratory Disease (Network-2). The line and arrows represent functional and physical interactions (solid line: direct; dotted lines: indirect link) and the direction of regulation as indicated in the literature. Empty nodes indicate genes not included in shared gene list while colored nodes indicate input genes for the network analysis. Upregulated and downregulated genes are indicated by red and green respectively.

**Table S1 Top 10 networks altered in *Pals1* CKO identified by IPA pathway analysis**

| ID.Network | Molecules in Network | Score | FG | Top Diseases and Functions |
|---|---|---|---|---|
| 1 | 14-3-3,ACTN1,CDC6,CDC25C,CDK2,CDT1,CHRNA3,Cyclin A,Cyclin E,E2f,E2F1,E2F2,EOMES,GDF15,HIST1H2AB/HIST1H2AE,HIST1H3A (includes others),ITGA7,KIF15,MCM3,MCM5,MCM6,MCM7,MCM10,MYBL2,NASP,NFkB (complex),NUSAP1,PDLIM1,PELI2,Rb,SKP2,TNFAIP8,TOP2A,TPX2,TYMS | 44 | 28 | Cell Cycle, DNA Replication, Recombination, and Repair, Cellular Assembly and Organization |
| 2 | ACTL6A,Alpha catenin, AURKA,BIRC5,BUB1B,CACNA1H,Ccnb1/Gm5593,Cdc2,CDC20,CDCA8,CDK1,CDKN1A,CHAF1B,Cyclin B,DLGAP5,EGR1,Hdac,HEY1,Histone H1,Histone h3,Histone h4,Hsp90,LBR,Lyz1/Lyz2,MMP2,NCAPD2,NDC80,Notch,P38 MAPK,PBK,PDGFRA,Ras homolog,RRM1,SPC25,ZEB2 | 33 | 24 | Cell Cycle, Cancer, Respiratory Disease |
| 3 | BUB1B,CBFA2T3,CD63,CDCA3,CENPA,CENPE,CLDN4,EBF2,ERBB2,FSTL3,G3BP1,GRB2,HIST1H2AD,KRT81,LEPR,LTBP3,MFAP4,MXD3,NCAPD2,NDC80,POLD1,PRC1,RFC4,RHOD,RNASET2,RPL30,SMTN,SP5,SPOCK1,STK17B,TGFB1,TOP2A,TP53INP1,YY1,ZWINT | 27 | 21 | Cancer, Reproductive System Disease, Cellular Assembly and Organization |
| 4 | Akt,Ap1,ARAF,Caspase 3/7,ELN,ERK1/2,FBLIM1,Filamin,Focal adhesion kinase,GAB1,GDNF,Gm-csf,HAS2,HIST2H3C (includes others),INPPL1,LDL,LOXL1,MAP2K1/2,Mapk,MDK,Mek,MMP9,OTX2,PDGF BB,Pkc(s),PRKD3,PTP4A3,Ras,SOCS3,SPHK1,SULF1,Tgf beta,UHRF1,ZFP36L1,ZFYVE21 | 25 | 20 | Cellular Movement, Renal and Urological System Development and Function, Connective Tissue Disorders |
| 5 | AK1,ANLN,CDC7,CDT1,CLSPN,COX6B2,CYP1A1,DBF4,EPHX1,FOXO1,GAMT,GPR17,HERC2,IDH2,KIAA0101,LDHA,MCM2,MCM5,MELK,miR-183-5p (miRNAs w/seed AUGGCAC),MVD,NCAPG,NEK2,PBK,POLD1,POLD2,PQLC3,PRC1,PTP4A3,RFC1,SCN | 25 | 20 | DNA Replication, Recombination, and Repair, Cancer, Gastrointestinal Disease |

| | | | | |
|---|---|---|---|---|
| | 3B,SIVA1,SLC19A2,SQLE,TP53 | | | |
| 6 | ADORA2A,ARNTL,ATOH1,AURKA,BMI1,CDC20,CDCA2,CRY1,CSF2,E2F7,E2F8,EED,EZH2,H1F0,HNRNPD,IFITM2,KCNB1,KIF23,KIF4A,MYT1,PHF1,PRC1,RACGAP1,RAD51,RAD54B,RAD54L,RECQL4,SAA2,SGOL1,SMC2,SPAG5,ST18,TCF12,TERC,UBD | 22 | 18 | Cell Cycle, Cellular Movement, Organismal Survival |
| 7 | 26s Proteasome,ACTN1,CCNG1,CDK14,CNIH4,COL15A1,COL16A1,CTGF,DAB1,estrogen receptor,FBLIM1,FSH,GLI1,GNRH,GPR21,HBP1,Hist1h2ak,KIF1B,KRAS,Lh,LTBP3,MBD2,MECP2,NLK,PCDH10,Pdlim3,PDZRN3,PGRMC1,PTBP1,PTF1A,RASSF4,SH3BP4,SMARCA4,Sos,TK1 | 22 | 18 | Cellular Development, Cellular Growth and Proliferation, Embryonic Development |
| 8 | CCDC80,CCND1,CDC6,CDC37,CDC45,CDK4,CDK5RAP2,CDKN1C,CDKN2C,CDKN2D,CENPH,CENPN,FABP4,FGFR2,FGFR3,FRMD3,FZD7,GFAP,GLI3,KIF11,KIF2C,LIN28A,MYBL2,N-cor,NCAPH,NEUROG2,NFIX,PECAM1,SKP2,SMARCB1,SMARCD2,STARD4,TRIM28,TXNIP,ZIC1 | 20 | 17 | Cellular Growth and Proliferation, Cell Cycle, Cellular Function and Maintenance |
| 9 | Actin,BCR (complex),CCND2,CD3,Cg,EFS,ERK,FAS,GADD45G,Gamma tubulin,IgG,IgG1,Igg3,Igm,IL12 (complex),Immunoglobulin,Interferon alpha,Jnk,KLC1,LMNB1,MAP3K1,MSC,NFATC1,p85 (pik3r),PARP,PI3K (complex),RFX4,RND2,STK17B,TCR,TMPO,UNG,VAV3,Vegf,ZIC2 | 18 | 16 | Cellular Movement, Hematological System Development and Function, Humoral Immune Response |
| 10 | ARNT,BRAF,CARTPT,CCDC99,CD24,CDCA4,CPE,DEPDC1B,ESCO2,GDF15,GPER,HIF1A,HIST2H2AC,IGF2,IGFBP2,IGFBP3,IGFBPL1,KIF18A,KNTC1,MEN1,MGEA5,NCOA3,NEUROD1,PDGFB,Proinsulin,RAB27A,SPHK1,Sytl2,SYTL4,TCF19,TGFA,TUFT1,UROD,ZW10,ZWILCH | 16 | 15 | Cellular Assembly and Organization, Hair and Skin Development and Function, Cancer |

**Table S2 Transcription regulators inhibited or activated in *Pals1* CKO mice**

| Transcription regulators | Predicted State | p-value | number of genes in networks |
|---|---|---|---|
| E2F1 | Inhibited | 1.72E-13 | 45 |
| E2F3 | Inhibited | 3.45E-12 | 18 |
| E2F2 | Inhibited | 3.06E-10 | 15 |
| MYC | Inhibited | 4.00E-10 | 66 |
| CCND1 | Inhibited | 1.27E-09 | 29 |
| TBX2 | Inhibited | 4.12E-09 | 15 |
| FOXM1 | Inhibited | 1.02E-05 | 12 |
| GLI2 | Inhibited | 4.48E-04 | 10 |
| KLF5 | Inhibited | 1.68E-02 | 5 |
| ZNF217 | Inhibited | 1.93E-02 | 6 |
| STAT5B | Inhibited | 3.53E-01 | 6 |
| NUPR1 | Activated | 1.09E-15 | 53 |
| TP53 | Activated | 1.13E-15 | 95 |
| RB1 | Activated | 1.56E-15 | 37 |
| CDKN2A | Activated | 5.35E-13 | 34 |
| E2F6 | Activated | 1.26E-09 | 14 |
| RBL1 | Activated | 1.36E-08 | 14 |
| PAX6 | Activated | 3.26E-06 | 20 |
| CEBPA | Activated | 1.07E-02 | 21 |
| HIF1A | Activated | 2.89E-02 | 17 |
| RELA | Activated | 3.37E-01 | 12 |

**Table S3 Primers used for real time PCR**

| | | |
|---|---|---|
| CDT1 | CACCTTCAAGGACAGCATCA | GACACGTTCCACCAGGTTCT |
| E2F1 | ACTGTGACTTTGGGGACCTG | CAGAGGGTATGGATCGTGCT |
| MCM7 | CCCACTTTCATGCCTCTGAT | CCCACAGGAACTTGGTCACT |
| MCM10 | GGATGGAATGCTGAAGGAGA | GCTTTTCAGAGCCACAGGAG |
| GDF15 | CGAGTGTCCCCACCTGTATC | CCACTGTCTGTCCTGTGCAT |
| EOMES | GGAAATGGCTGGTTGCTAAA | TTCCTTCCTTCCTTCCTTCC |
| BUB1B | TTGTGCAATGAACCTTTGGA | CGTTCAATCCCTTCCTGAAA |
| CDC20 | AGACCACCCCTAGCAAACCT | GAGACCAGGCTTTCTGATGC |
| PBK | TTCCACACGTCAATCTTCCA | CAATGGCCTTCTGGTAGGAG |
| AurkA | ACCAGGCCTAGGGAAACTGT | CAGTGGCTGAGGATCCAAAT |
| PDGFRA | TGGCATGATGGTCGATTCTA | CGCTGAGGTGGTAGAAGGAG |
| Lyz1 | GTCACACTTCCTCGCTTTCC | TGACTGTCACCAGCATCCAT |
| CDKN1A | TATTTAAGCCCCTCCCAACC | TCACCCCCAGGTAAGAAGTG |
| Hey1 | TGATGGACCGAGGTGTTGTA | TCCCTTCACCTCACTGCTCT |
| LBR | ACCGAAAGGCTCCAGAAGAT | GTTGTACACGCTGACGCTGT |
| BIRC5 | TGGCAGCTGTACCTCAAGAA | AAAACACTGGGCCAAATCAG |
| Pals1 | CTTCGCACACAGTCCTTGAA | CTAACAACGCCCGAAGTCTC |
| 18s rRNA | GAATAATGGAATAGGACCGCGG | GGAACTACGACGGTATCTGATC |
| Actin | CTGAACCCTAAGGCCAACC | CCTGGATGGCTACGTACATG |